ORO-2504-291

PRODUCTION OF ULTRA-COLD NEUTRONS USING DOPPLER-SHIFTED BRAGG SCATTERING AND AN INTENSE PULSED NEUTRON SPALLATION SOURCE

by

T. W. Dombeck and J. W. Lynn
with University of Missouri and Argonne National Laboratory

PP No. 79-153

TR No. 79-085

March 1979

UNIVERSITY OF MARYLAND
DEPARTMENT OF PHYSICS AND ASTRONOMY
COLLEGE PARK, MARYLAND

PRODUCTION OF ULTRA-COLD NEUTRONS USING DOPPLER-SHIFTED BRAGG SCATTERING AND AN INTENSE PULSED NEUTRON SPALLATION SOURCE

by

T. W. Dombeck and J. W. Lynn
with University of Missouri and Argonne National Laboratory

PP No. 79-153

TR No. 79-085

March 1979

Production of Ultra-Cold Neutrons Using Doppler-Shifted Bragg Scattering and an Intense Pulsed Neutron Spallation Source

T. W. Dombeck and J. W. Lynn

University of Maryland, College Park, Maryland 20742

S.A. Werner

University of Missouri, Columbia, Missouri 65201

T. Brun, J. Carpenter, V. Krohn, and R. Ringo

Argonne National Laboratory, Argonne, Illinois 60439

We present an analytic and a computer generated simulation of the production of Ultra-Cold Neutrons (UCN) using Bragg scattering from a moving crystal to Doppler shift higher velocity neutrons into the UCN region. The calculation was carried out with a view toward its application at the Intense Pulsed Neutron Source (IPNS) now under construction at Argonne National Laboratory. This method for the production of UCN appears well matched to a pulsed source, and we show that the UCN can be stored in a neutron bottle at the peak flux which can potentially be much higher than at the present high flux reactors. The predicted density of stored UCN indicates that a highly precise measurement of the neutron electric dipole moment (EDM) will be possible within the next few years.

I. INTRODUCTION

Methods to produce Ultra-Cold Neutrons (UCN) have aroused considerable interest in recent years as potentially providing a means to carry out a very precise search for the electric dipole moment (EDM) of the neutron.[1-6] The reason for this is that UCN can be confined in a "bottle" for long periods of time, thus increasing the measuring time and hence the sensitivity to the neutron EDM by perhaps as much as four orders of magnitude.[7-8] In this paper we describe a technique in which UCN are generated by Doppler-shifting cold neutrons[4,9,10,11] ($\sim$10Å) produced in a pulsed neutron source, down to ultra-cold velocities using Bragg reflection from a moving crystal. We show that the density of UCN which can be stored in a bottle is limited by the peak density in the source, and not by the time-averaged density. For this reason the pulsed neutron source appears very attractive for this application since peak fluxes exceeding 10^{16} n/cm^2-s are expected to become available within a few years.[12]

The observation of a neutron electric dipole moment would be the first example in which P and T symmetries were violated in a particle interaction. CP nonconservation was observed in the K_L^o - $\bar{K}_L^o$ decay system,[13] and many theories attempting to explain CP violation predict, as a consequence of the CPT theorem, a finite neutron EDM. Stimulated by this theoretical speculation, a number of precision experiments employing magnetic-resonance spectrometers have searched for the neutron EDM. The most recent measurement places an upper limit on its existence of 3×10^{-24} e-cm.[14-15] This limit has already eliminated many theories which predicted larger EDM values, however, a few exceptions remain. Among them is the prediction[16]

containers. The most recent UCN beam at the high flux reactor at the Institute Max Von Laue - Paul Langevin (ILL), Grenoble, France is capable of storing neutrons with a density of one per cm^3.[5] A neutron bottle experiment has been proposed using this beam to perform an EDM measurement with a precision of 10^{-26} e-cm.[28]

The UCN source described in this paper is currently under construction and will be used in conjunction with the Argonne National Laboratory Intense Pulsed Neutron Source (IPNS).[12] This source produces short bursts of fast neutrons from a spallation target bombarded by high energy protons (500-1000 MeV). The neutrons are then slowed in a hydrogenous moderator. The planned UCN facility will take advantage of the peak flux from the moderator to fill a bottle by Doppler shifting pulses of neutrons from a velocity of about 400 m/s down to the UCN region (0 to 7 m/s) using Bragg reflection from a moving mica crystal. A shutter will let neutrons into the bottle when the pulses arrive and close the bottle between pulses. In this way the bottle is filled by many pulses as if by a steady beam at the peak flux. The pulsed nature of the source results in a relatively unimportant increase in the filling time ($\sim$ one minute) compared to that necessary at a steady-state source.

In the following section we present a brief description of the apparatus and the experimental arrangement. In section III we will discuss analytically the effectiveness of Doppler shifting cold neutrons down to ultracold velocities while in section IV we will treat this same problem using numerical Monte Carlo methods. The main advantage of doing this problem analytically is that we can more easily examine the qualitative dependence of the efficiency of producing and utilizing Ultra-Cold Neutrons

on the various experimental parameters. However, in order to carry the analytic calculation to completion, it is necessary to make certain approximations which are not necessary in the numerical treatment. Agreement between the results of these two approaches has added significant confidence in our estimates of the Ultra-Cold Neutron storage density achievable at the Intense Pulsed Neutron Source.

II. APPARATUS AND BEAM CHARACTERISTICS

The Doppler Shifter Assembly is shown in Fig. 1. Neutrons leaving the spallation target are cooled by a cold hydrogenous moderator (10 X 10 X 5 cm^3)at 20°K. The calculation of the neutron flux leaving the moderator involves specifics about the arrangement of the target and the moderator. However, it appears that with the proper placement of the moderator a time average thermal flux $\bar{\Phi}$ of 6 X 10^{11} n/cm^2-s will be available at IPNS-I.[12] The peak of the velocity distribution v_T for a similar type of moderator has been measured to be 650 m/s[29] and the pulse width τ is expected to be 200 μs and not to change much down to a velocity of 395 m/s.

The neutrons from the moderator travel through the shielding wall in a beam tube containing He gas at room pressure (diameter ∿10cm). This tube can be constructed to act as a beam guide. The Doppler shifting crystal is mounted in a vacuum near the edge of a rotor operating at the same frequency and in phase with the arrival of neutrons from the moderator (30 Hz for IPNS). The rotational sense is such that the crystal moves away from the source when it is in the incident beam. The tangential velocity $\vec{v}_R$ and the angle at which the crystal is mounted is set by the Bragg condition and the velocity space volume to be reflected as UCN.

After Doppler shifting, the UCN enter part of the bottle facility through a shutter device arranged close to the edge of the rotor. The shutter opens and closes in phase with the passing crystal and traps the

neutrons in the bottle. After many pulses the bottle will arrive asymptotically at the maximum density of stored neutrons; i.e., when the number entering through the shutter equals the number of neutrons lost between pulses.

The neutron bottle is capable of storing neutrons up to a certain velocity (v_{MAX}) which is determined by the limiting wavelength at which total internal reflection[6] occurs off the walls. (In Table I we have listed a number of wall materials and their values of v_{MAX}.) Owing to component mixing on reflection from the walls the acceptance of the bottle in velocity space is approximately a sphere with a volume $4\pi v_{MAX}^3/3$. The velocity space volume reflected by the crystal should match this acceptance.

The shutter consists of an auxiliary rotating disk perpendicular to the rotor and in phase with it. A slot cut in the disk periodically opens the bottle entrance. The parameters for the source, rotor, crystal, and the shutter that will be used at Argonne Laboratory are given in Table II.

The average phase space density $\bar{n}(\vec{v})$ at the source can be computed from the time average flux and is given by

$$\bar{n}(\vec{v}) = \bar{\phi} \frac{1}{2\pi v_T^4} e^{-(v/v_T)^2} \qquad (1)$$

where v_T is the mean velocity corresponding to the moderator temperature ($\frac{1}{2} mv_T^2 = kT$). Using the values for $\bar{\phi}$ and v_T given above, the time average phase space density is 0.004 $n/cm^3\text{-}(m/s)^3$ for IPNS-I. The peak phase space density is found by dividing (1) by the duty factor $f\Delta\tau$, where f is the frequency of pulses (30 Hz) and the $\Delta\tau$ is the effective pulse width ($\sim$200 μs, FWHM) yielding

$$n_p(\vec{v}) = 0.66 \text{ n/cm}^3 - (\text{m/s})^3 \qquad (2)$$

It is useful to calculate the maximum peak density of neutrons available for containment as a figure of merit to compare with the final stored density. The region of phase space which can be shifted from a velocity around 395 m/s to the UCN range has a volume given by $4\pi v_{MAX}^3/3$. The density of neutrons in this region follows from (2)

$$\rho_{MAX} = n_p \frac{4}{3} \pi v_{MAX}^3 \simeq 10^3 \text{ n/cm}^3 \quad \text{(for IPNS-I)} \qquad (3)$$

According to Lioville's theorem we cannot exceed (3) in the final bottle density. Furthermore, this result is decreased by various inefficiencies which arise in the Doppler-shifting and collection process. In the following sections we attempt to identify and calculate these inefficiencies.

III. ANALYTICAL TREATMENT OF THE DOPPLER-SHIFTER

The main physical characteristics of Bragg reflection by a moving crystal are well-known and have been checked experimentally.[9,10,11,30,31,32,33] The difficulty in applying the results of these papers directly to our problem arises from the fact the incident beam is pulsed and that the crystal is both rotating and translating. The analysis presented here is based on the geometrical opportunities and constraints achievable at the pulsed neutron source IPNS-I scheduled to begin operation at the Argonne National Laboratory in 1980.

A. Velocity Transformations

Consider a crystal mounted rigidly to a rotor of radius R rotating with angular frequency ω as shown in Fig. 2. The reflecting planes in the crystal are set at an angle β with respect to the local radius vector $\vec{R}$ of the rotor (see Fig. 2a). The angle between the velocity vector $\vec{v}_R$ and the central ray of the incident beam is also β when the crystal passes the beam center. It is important that this angle is not zero, as we shall see.

If we Bragg reflect neutrons of laboratory velocity $\vec{v}_{nL}$ from a crystal moving with velocity $\vec{v}_R$, the effective incident velocity of the neutron in the moving system is

$$\vec{v}_{nR} = \vec{v}_{nL} - \vec{v}_R \quad . \tag{4}$$

The velocity of the reflected neutrons in the moving system is determined by the Bragg relation

$$\vec{v}'_{nR} = \vec{v}_{nR} + \frac{\hbar}{m}\vec{G} \quad , \tag{5}$$

where $\vec{G}$ is the reciprocal lattice vector corresponding to the reflecting planes ($|\vec{G}| = \frac{2\pi}{d}$), and the magnitude of the incident and reflected velocity vectors in the moving coordinate frame must be equal,

$$|\vec{v}'_{nR}| = |\vec{v}_{nR}| \quad . \tag{6}$$

The laboratory velocity of the reflected neutrons is then

$$\vec{v}'_{nL} = \vec{v}'_{nR} + \vec{v}_R \quad . \tag{7}$$

It should be noted that the above equations require

$$\vec{v}'_{nL} = \vec{v}_{nL} + \frac{\hbar}{m}\vec{G} \quad . \tag{8}$$

A velocity-vector diagram of these equations is shown in Fig. 2b. It will be noted from this diagram that the reflected neutron velocity in the laboratory frame $\vec{v}'_{nL}$ is zero when the incident velocity $\vec{v}_{nL}$ is directed anti-parallel to the reciprocal lattice vector $\vec{G}$ and equal in magnitude to $\frac{\hbar}{m}G$. This condition can, in principle, be met for any crystal. However, in order to keep the tangential velocity of the rotor down to some reasonable speed, it is desirable to select a crystal for which G is fairly small. This requires choosing a crystal which has as large a plane spacing d as possible. In terms of availability, strength and neutron reflectivity properties, synthetic mica seems to be the optimum choice. Another consideration is also important: in order to utilize a reasonable beam area there will necessarily be a gradient of the velocity $\vec{v}_R$ across the surface of the crystal. Consequently, the condition for Doppler-shifting neutrons down to near zero velocity can only be met for some fraction of the crystal area at a given instant of time. This velocity gradient is, of course, smaller the lower $\vec{v}_R$, which also requires $\vec{G}$ to be as small as possible. On the basis of the numbers for a rotor of practical dimensions, this consideration seems to rule out the commonly used neutron monochromators Cu, Be, and pyrolytic graphite for this application.

B. Effective Volumes in Velocity Space

Since the crystal is necessarily imperfect, having a mosaic structure, and the incident beam is divergent and polyenergetic, we must inquire about the volume of neutrons in velocity space actually reflected by the crystal. In fact, we need to know this volume at each instant of time t, and at each position (x,y) on the crystal face. We need also to calculate the intersection or overlap of this volume in velocity space with a sphere of radius v_{MAX} centered at $\vec{v}'_{nL} = 0$. It is only neutrons within this sphere which are termed Ultra-Cold and can be stored in the neutron bottle.

Suppose the phase of the rotor is such that the center of the crystal is in the center of the beam when the center of the neutron pulse of wavelength $\lambda_{nL} = \lambda^{\circ}_{nL}$ (= 9.96 Å for mica) arrives at the crystal. Call this time t = 0. Consider also, only the center point of the crystal (x=0,y=0) for now. Take point 0 to be the center of neutron velocity space as shown in Fig. 3. The crystal will reflect neutrons of incident velocity $\vec{v}_{nR}$ in the moving frame in the velocity-space volume B into the volume B' with an average efficiency decreasing with increasing distance for the centroid of B. The volume of incident neutrons as viewed in the laboratory frame corresponding to the volume B is labelled A in this figure. Transforming reflected neutron velocities within B' back to the laboratory frame leaves them within the volume C centered at $\vec{v}'_{nL} = 0$. The Bragg angle in the frame of the moving crystal is θ_B. The dimensions of these volumes can be obtained from standard monochromator theory.[34] The dimensions of each of these volumes in the v_x-v_z plane are equal, as shown in Fig. 3. If we assume that the transmission function of the collimator is Gaussian, and that the reflectivity of the crystal is also Gaussian, then

$$W_x = v^{\circ}_{nL}\, \alpha_x \,, \qquad (9)$$

and

$$W_z = v_R^\circ \eta_x \sin\beta = \frac{1}{2} v_{nL}^\circ \eta_x \tan\beta \quad . \qquad (10)$$

In the direction perpendicular to the plane of Fig. 3, the volumes A and B are of height $v_{nL}^\circ \alpha_y$, while the y-dimension of volumes B' and C is

$$W_y = v_{nL}^\circ \sqrt{\eta_y^2 + \alpha_y^2} \quad . \qquad (11)$$

Here α_x and α_y are the Gaussian parameters specifying the in-plane and out-of-plane collimations, while η_x and η_y are the in-plane and out-of-plane Gaussian mosiac spread parameters. The numerical factor 2.35 ($= 2\sqrt{2\ell n 2}$) relates the Gaussian parameters to the full-width-at-half maximum (FWHM) in Fig. 3 of each of these distributions. Thus, the boundaries of the volumes shown in Fig. 3 are meant to be 50% contours of probability. They are actually ellipsoids. The superscripts on $\vec{v}_{nL}^\circ$ and $\vec{v}_R^\circ$ indicates the nominal values of $\vec{v}_{nL}$ and $\vec{v}_R$.

The heights of the volumes B' and C are larger than those of the volumes A and B because the out-of-plane mosaic spread of crystal broadens the distribution of neutrons upon reflection in the y-direction. In fact, aside from a loss of neutron density due to the efficiency of Bragg reflection, the density of neutrons in velocity space is decreased by the ratio

$$r = \frac{\alpha_y}{\sqrt{\eta_y^2 + \alpha_y^2}} \qquad (12)$$

due to this effect. It is therefore clear that it is desirable to make the out-of-plane mosaic spread η_y small in comparison to the out-of-plane collimation α_y. From eqs. (9), (10), and (11) we see that the volume C of neutrons in velocity space resulting from Bragg reflection is

$$(\text{vol})_C = (2.35)^3 W_x W_y W_z = \frac{1}{2}(2.35)^3 \alpha_x \eta_x \sqrt{\alpha_y^2 + \eta_y^2}\,(v_{nL}^\circ)^3 \tan\beta \quad . (13)$$

The reflected intensity will be proportional to this volume and will therefore be zero at $\beta = 0$. Thus, direct back reflection in the moving frame will give zero intensity. (There will be a vanishingly small backward intensity due to the Darwin width, but no contribution from the crystal mosaic spread.)

C. Numerical Values of Parameters

Before proceeding with a detailed analysis of the reflection efficiency as a function of time t and position (x,y) on the crystal face, we will first attempt to provide some qualitative feeling for the parameter involved. If we choose mica as the Doppler-shifting monochromator crystal, then the nominal incident neutron wavelength and velocity in the laboratory frame are:

$$\lambda_{nL}^\circ = d_{mica} = 9.96\ \text{Å}\ , \qquad (14a)$$

and

$$v_{nL}^\circ = 395\ \text{m/sec}\ . \qquad (14b)$$

The Bragg angle is chosen to be 61.2° giving a β of 28.8°. This angle was chosen in order to have reflected a reasonable velocity space volume as given by eq. (13) while keeping the rotor design within practical limits. An optimal value of β would be 37° which yields an increase of 20% in velocity space volume at the expense of a higher rotor tangential velocity.

Using $\beta = 28.8°$, and the arrangement shown in Fig. 3 we find

$$v_{nR}^\circ = v_R^\circ = 225.4\ \text{m/sec} \qquad (14c)$$

If we phase the rotor to the pulsed source which operates at 30 Hz, then

the radius of the rotor should be

$$R = v_R^\circ/\omega = 1.202 \text{ m.} \qquad (15)$$

Thus, the crystal will arrive back in the incident beam when the next pulse of neutrons comes from the source.

It is clear that we should choose the parameters α_x, α_y, η_x, and η_y so that the dimensions of the volume C in velocity space are comparable to the size of a spherical volume of radius equal to the maximum velocity neutron which can be stored in a bottle. For a bottle made of Be this velocity is $v_{MAX} = 7$ m/sec. To be explicit, suppose that the source area is $W_s \times W_s = 8.86$ cm X 8.86 cm and the crystal can be placed a distance $L_o = 4.8$ m from the source; then

$$2.35\ \alpha_x = 2.35\ \alpha_y = \frac{W_s}{L} = 0.0185 \text{ rad.} = 1.06^\circ . \qquad (16)$$

Suppose also that the crystal has a mosaic width (FWHM) of

$$2.35\ \eta_x = 0.052 \text{ rad.} = 3^\circ \qquad (17)$$

The dimensions of the velocity space volumes as given by equations (9), (10), and (11) are then

$$\begin{aligned} 2.35\ W_x &= 7.31 \text{ m/sec.} \\ 2.35\ W_y &= 8.08 \text{ m/sec.} \\ 2.35\ W_z &= 5.65 \text{ m/sec.} \end{aligned} \qquad (18)$$

We have assumed $2.35\ \eta_y$ to be $1/2^\circ$. We therefore see that W_x, W_y, and W_z can be made comparable to $2v_{MAX} \approx 14$ m/sec with reasonable values of the collimation parameters and the mosaic spread parameters. It is clear from these numbers that it would be advantageous to be closer to the source (than $L_o = 4.8$ m), or to use a beam guide to aid in bringing the source out to the crystal.

There is another important preliminary numerical consideration: the crystal should remain in the incident beam for a large fraction of the time that neutrons of velocities within the sphere of radius v_{MAX}, centered at $\vec{v}^{\circ}_{nL}$, are arriving from the source. The pulse width at the source for neutrons of velocity v°_{nL} = 395 m/sec is projected to be about[12,29]

$$\tau_{source} = 200 \text{ μsec.} \tag{19}$$

The difference in arrival times (at the crystal) of neutrons of velocities $v^{\circ}_{nL} + v_{MAX}$ and $v^{\circ}_{nL} - v_{MAX}$ for L_o = 4.8 m is

$$\Delta t_{arrival} = \frac{L_o}{v^{\circ}_{nL} + v_{MAX}} - \frac{L_o}{v^{\circ}_{nL} - v_{MAX}} \simeq \frac{2L_o}{(v^{\circ}_{nL})^2} v_{MAX} = 395 \text{ μsec.} \tag{20}$$

Thus, neutrons which are potentially useful for storage in a bottle will be arriving at the crystal over a time span

$$\tau_{total} = \tau_{source} + \Delta t_{arrival} = 595 \text{ μsec.} \tag{21}$$

The transit time of the center of the crystal across the beam of width W = 8.86 cm is

$$\Delta t_{transit} = \frac{W/\sin\beta}{v^{\circ}_{R}} = 773 \text{ μsec.} \tag{22}$$

We therefore conclude that the transit time of the crystal across the beam is sufficiently long to utilize all those neutrons arriving at the crystal location which are of velocities suitable for storage upon being Doppler-shifted down in velocity.

D. Motion of the Center of the Velocity Space Volume

We continue now to fix our attention on the center of the crystal at x = 0, y = 0 (the origin of x,y coordinates is fixed to the crystal).

As a function of time, this point moves across the beam. We will now calculate the "trajectory" of the center of the velocity space volume C in velocity space as a function of time t. We first note that during the time interval τ_{total}, the orientation of the crystal has changed by an angle $\omega\tau_{total} = 6.4°$. Thus, the vector $\vec{G}$ will have rotated by this same angle. The effect of this rotation on the shape of the velocity space volumes of Fig. 3 is very small, and will be neglected. However, the centers of these volumes will move as a function of time due to the rotation of $\vec{G}$. This is an important effect.

Let the symbol $\vec{V}_{nL}(t)$ describe the position of the center of volume A as a function of time. (At t = 0, $\vec{V}_{nL}(t) = \vec{v}^{\circ}_{nL}$.) Similarly, let $\vec{V}_{nR}(t)$, $\vec{V}'_{nR}(t)$, and $\vec{V}'_{nL}(t)$ describe the position of the center of the volumes B, B', and C as a function of time respectively. According to eq.(4) we must have

$$\vec{V}_{nR}(t) = \vec{V}_{nL}(t) - \vec{V}_{R}(t). \tag{23}$$

Thus, the change in these velocity vectors, describing the centroids of volumes A, B, and B' are related by

$$\Delta\vec{V}_{nR} = \Delta\vec{V}_{nL} - \Delta\vec{V}_{R}. \tag{24}$$

The magnitude of the velocity vector $\vec{V}_R$ is constant; however, the direction of $\vec{V}_R$ changes as the rotor turns. From geometry, we find

$$\Delta\vec{V}_{R} = \omega t v^{\circ}_{R}[-\cos\beta\,\hat{x} + \sin\beta\,\hat{z}]. \tag{25}$$

We now resolve the vector $\Delta\vec{V}_{nL}$ into components:

$$\Delta\vec{V}_{nL} = \Delta V_{nLx}\,\hat{x} + \Delta V_{nLy}\,\hat{y} + \Delta V_{nLz}\hat{z}\ . \tag{26}$$

It is clear that for the center point of the crystal (x = 0, y = 0), which

is under consideration now, that

$$\Delta V_{nLy} = 0 \quad . \tag{27}$$

Since the center of the crystal has moved a distance $v^{\circ}_{Rx}t$ in a time t in the x-direction, we can calculate the change in V_{nLx} with the aid of Figs. 2a and 3. By similar triangles, constructed in real space (Fig. 2a) and velocity space (Fig. 3), we have

$$\frac{\Delta V_{nLx}}{v^{\circ}_{nL}} = \frac{v_{nRx}t}{L_o} \quad . \tag{28}$$

Therefore,

$$\Delta V_{nLx} = \frac{(v^{\circ}_{R}\sin\beta)t}{L_o}\ v^{\circ}_{nL} \quad , \tag{29}$$

where L_o is the distance from the source to the center of the crystal at $t = 0$. We now know the $\hat{x}$ and $\hat{y}$ components of the vector $\Delta\vec{V}_{nL}$. We will now show that the $\hat{z}$ component is zero. At any time t, the centroids of the volumes B and B' are connected by the vector $\frac{\hbar\vec{G}}{m}$ (Bragg's Law); therefore

$$\vec{V}'_{nR}(t) = \vec{V}_{nR}(t) + \frac{\hbar}{m}\vec{G}(t), \tag{30}$$

and

$$\Delta\vec{V}'_{nR} = \Delta\vec{V}_{nR} + \frac{\hbar}{m}\Delta\vec{G}. \tag{31}$$

The length of the vector $\vec{G}$ is fixed. The change $\Delta\vec{G}$ comes from the rotation of the crystal, namely

$$\Delta\vec{G} = \omega t G\hat{x} \ . \tag{32}$$

If we square both sides of eq. (30) and recall that Bragg scattering in the moving frame is elastic, that is

$$V'^{2}_{nR} = V^{2}_{nR}, \tag{33}$$

we then have

$$2\vec{V}_{nR} \cdot \vec{G} + \frac{\hbar}{m} G^2 = 0. \tag{34}$$

The variation of this equation gives

$$\vec{v}^{\,\circ}_{nR} \cdot \Delta\vec{G} + \Delta\vec{V}_{nR} \cdot \vec{G}^{\circ} + \frac{\hbar}{m} \Delta\vec{G} \cdot \vec{G}^{\circ} = 0 \tag{35}$$

The last term of this equation is zero, since $\Delta\vec{G}$ (eq. 3?) is perpendicular to $\vec{G}^{\circ} = -G\hat{z}$. Writing out the components of the remaining dot products, we find

$$\Delta V_{nRz} = -\frac{v^{\circ}_{nRx}}{G} \Delta G_x = -v^{\circ}_R \sin\beta\ \omega t, \tag{36}$$

where we have used eq. (32) and the fact $v^{\circ}_{nR} = v^{\circ}_R$. Equating the $\hat{z}$-components of eq. (24), we have

$$\Delta V_{nLz} = \Delta V_{nRz} + \Delta V_{Rz} \quad . \tag{37}$$

From eqs. (25) and (36) we see that

$$\Delta V_{nRz} = -\Delta V_{Rz} \quad , \tag{38}$$

so that finally we have

$$\Delta V_{nLz} = 0. \tag{39}$$

Consequently, the centroid of the volume A moves in the $\hat{x}$ direction in velocity space, namely

$$\Delta\vec{V}_{nL} = \frac{(v^{\circ}_R \sin\beta)t}{L_o}\ v^{\circ}_{nL}\ \hat{x} \quad . \tag{40}$$

We need to use this result to find $\Delta\vec{V}'_{nL}$. This is easily done, since

$$\Delta\vec{V}'_{nL} = \Delta\vec{V}_{nL} + \frac{\hbar}{m} \Delta\vec{G}. \tag{41}$$

Using the fact that $v^{\circ}_{nL} = \frac{\hbar}{m} G$, and eqs. (32) and (40) we find

$$\Delta\vec{V}'_{nL}(t) = \left(\frac{v^{\circ}_R \sin\beta}{L_o} + \omega\right)t\ v^{\circ}_{nL}\ \hat{x} \quad . \tag{42}$$

This is a very important result. It tells us that the distribution of Doppler-shifted neutrons in velocity space moves only in a direction perpendicular to the incident beam as the rotor turns. To obtain a feeling for the size of this shift, suppose again that L_o = 4.8 m, β = 28.8°, $\omega = 2\pi(30)$ rad/sec, and v°_{nL} = 395 m/sec; then $|\Delta v'_{nL}|$ = 8.34 m/sec at t = 100 μsec. Thus, we see the centroid of the ultracold velocity distribution has shifted beyond $v_{MAX} \approx 7$ m/sec at a time t = 100 μsec. However, this is only for the center point on the crystal surface. Other points (x,y) on the crystal will become increasingly important for various other times t. The overlap of the Doppler-shifted reflected volume C with a sphere of radius v_{MAX} at various times at x = 0, y = 0 is shown in Fig. 4a. The formulas for calculating the overlap at other positions (x,y) are derived in the next section. The time evolution of the overlap volume at x = 2 cm, y = 0 is shown in Fig. 4b.

E. Other Points (x,y) on the Crystal Face

We now wish to generalize the result for $\Delta\vec{V}'_{nL}$ given by eq. (42) to an arbitrary point (x,y) on the crystal face. We again resolve $\Delta\vec{V}_{nL}$ into components as in eq. (26). From geometry, it is apparent that

$$\Delta V_{nLy} = \frac{y}{L_o} v^\circ_{nL} \quad . \tag{43}$$

Using geometrical arguments identical to those leading to eq. (29), we find that

$$\Delta V_{nLx} = \frac{(v^\circ_R \sin\beta)t + x}{L_o} v^\circ_{nL} \quad . \tag{44}$$

We now need to find Δy_{nLz}, which will turn out to be non-zero in this case. Because we are considering a point (x,y) on the crystal which is further out on the rotor at, say

$$R = R_o + \Delta R = R_o + x\cos\beta, \tag{45}$$

the difference between $\vec{V}_R$ and $\vec{v}_R^{\,o}$ is now

$$\Delta\vec{V}_R = v_R^o\,[-\cos\beta\,\hat{x} + \sin\beta\,\hat{z}]\,\omega t + \omega x\cos\beta[\cos\beta\,\hat{x} + \sin\beta\,\hat{z}]. \tag{46}$$

The arguments leading to the expression for ΔV_{nRz} given by eq. (36) are valid for all points (x,y). Thus, we have, using eqs. (36) and (46), the result for ΔV_{nLz}:

$$\Delta V_{nLz} = \Delta V_{nRz} + \Delta V_{Rz} = \omega x\cos\beta\sin\beta = \frac{\omega x}{2}\sin 2\beta\ . \tag{47}$$

Eqs. (43), (44), and (47) are the components of the vector $\Delta\vec{V}_{nL}$; therefore, using eq. (41) and eq. (32) we have

$$\Delta\vec{V}'_{nL}(t) = v_{nL}^o\left[\frac{(v_R^o\sin\beta)t + x}{L_o} + \omega t\right]\hat{x} + \frac{y}{L_o}\,v_{nL}^o\,\hat{y} + \frac{\omega x}{2}\,\sin 2\beta\,\hat{z}. \tag{48}$$

This expression is the generalization of eq. (42) we have sought. $\Delta\vec{V}'_{nL}$ here, gives the position of the centroid of the velocity-space distribution of Ultra-Cold Neutrons generated by Doppler-shifted Bragg scattering for each time t, and for each position (x,y) on the crystal face.

F. The Efficiency of the Doppler Shifter, ε_{DS}

The phase space density of neutrons n_o incident on the crystal is the same when viewed in the laboratory frame as when viewed in the frame of reference fixed to the moving crystal, that is

$$n_o = n_o(\vec{r}_L,\ \vec{v}_{nL},\ t) = n_o(\vec{r}_R,\ \vec{v}_{nR},\ t)\ . \tag{49}$$

In the moving frame, the incident current density is

$$\vec{J}_{nR}(\vec{r}_R, \vec{v}_{nR}, t) = \vec{v}_{nR}\, n_o(\vec{r}_R, \vec{v}_{nR}, t) \quad . \tag{50}$$

The reflected current density in the moving frame is

$$J'_{nR}(\vec{r}_R, \vec{v}'_{nR}, t) = \varepsilon_{DS}\, J_{nR}(\vec{r}_R, \vec{v}_{nR}, t). \tag{51}$$

This equation defines the efficiency of the Doppler-shifter. Under the Gaussian approximations we have assumed for the mosaic structure of the crystal, and the collimator transmission function, ε_{DS} is simply given by the probability contours of the volume B' of Fig. 3. That is

$$\varepsilon_{DS}(\delta\vec{v}'_{nR}) = r\gamma_o \exp\{-1/2(\delta v'_{nRx}/W_x)^2 - 1/2(\delta v'_{nRy}/W_y)^2 - 1/2(\delta v'_{nRz}/W_z)^2\},$$

where (52)

$$\delta\vec{v}'_{nR} \equiv \vec{v}'_{nR}(t) - \vec{v}'_{nR}(0) - \Delta\vec{V}_{nR}(t), \tag{53}$$

γ_o is the unintegrated peak reflectivity of the crystal and r is given by (12). The efficiency ε_{DS} can equally well be expressed in terms of the velocity $\vec{v}'_{nL}$ of the reflected neutrons in the laboratory frame:

$$\varepsilon_{DS}(\vec{v}'_{nL}) = r\gamma_o \exp\{-1/2(v'_{nLx} - \Delta V'_{nLx})^2/W_x^2 - 1/2\,(V'_{nLy} - \Delta V'_{nLy})^2/W_y^2 - 1/2(v'_{nLz} - \Delta V'_{nLz})^2/W_z^2\}. \tag{54}$$

This form will prove more useful to us than eq. (52). It should be noted that ε_{DS} is also a function of x,y,t, since the location of the centroid $\Delta\vec{V}'_{nL}$ is explicitly a function of these parameters as given in eq. (48).

G. The Incident Neutron Phase Space Density n_o

If we approximate the neutron source pulse by a Gaussian function in time, having a FWHM = τ, then the phase space density of neutrons arriving at the crystal will be:

$$n_o(\vec{r}_L, \vec{v}_{nL}, t) = n_p \, e^{-1/2 \left\{ [t + \frac{L_o \, \delta v_{nLz}}{(v^o_{nL})^2}]^2 / (\tau/2.35)^2 \right\}} \quad (55)$$

Here δv_{nLz} gives the difference between the beam-line velocity of a given incident neutron in the laboratory frame and the nominal incident velocity v^o_{nL}, that is

$$\delta v_{nLz} = v_{nLz} - v^o_{nL} \quad (56)$$

The peak neutron phase space density is n_p. The factor $L_o \, \delta v_{nLz}/(v^o_{nL})^2$ in the exponent of the expression (55) accounts for the fact that incident neutrons of velocity greater than the nominal velocity v^o_{nL} arrive at the crystal at earlier times. From the geometry of Fig. 3 it is easy to show that

$$\delta v_{nLz} = v'_{nLz}. \quad (57)$$

Thus, we can express n_o in terms of the reflected neutron velocities in the laboratory frame.

H. The Source Density of Ultra-Cold Neutrons $\vec{S}_{u.c.}$

The current density $\vec{J}'_{nR}$ given by eq. (51) should be viewed as the source density $\vec{S}$ for Doppler-shifted neutrons. It gives the number of neutrons "emitted" at the point (x,y) on the surface of the crystal per cm^2 per sec at a time t per unit volume in velocity space. Each of these neutrons appears as a very slow neutron when viewed in the laboratory frame of reference. That is, the magnitude of the source vector $\vec{S}$ is the same in

both the moving frame and the laboratory frame, only its direction is changed due to the coordinate transformation. Thus, we have

$$\vec{S} = \frac{\vec{v}'_{nL}}{v'_{nL}} \epsilon_{D.S.} \, v_{nR} \, n_o \quad . \tag{58}$$

or, using eqs. (51), (54), and (55) we see that

$$\vec{S} = \frac{\vec{v}'_{nL}}{v'_{nL}} r\gamma_o e^{-1/2[(v'_{nLx} - \Delta V'_{nLx})^2/W_x^2 + (v'_{nLy} - \Delta V'_{nLx})^2/W_y^2 + (v'_{nLz} - \Delta V'_{nLz})^2/W_z^2]}$$

$$x \, v_R^o \, n_p \, e^{-1/2[t + \frac{L_o v'_{nLy}}{(v^o_{nL})^2}]^2/(\tau/2.35)^2} \tag{59}$$

In going from eq. (58) to (59) we have replaced v_{nR} by its nominal value which is equal to the nominal rotor velocity v_R^o as can be seen from Fig. 3.

Only neutrons having speeds below some maximum speed v_{max} can be stored in the bottle. We then are interested in

$$\vec{S}_{u.c.} = \int_{\substack{\text{sphere} \\ \text{of radius} \\ v_{max}}} \vec{S} \, d^3\vec{v}'_{nL} \quad . \tag{60}$$

Instead of assuming there is a precise cutoff speed v_{max} we will approximate the neutron bottle capture probability by a Gaussian:

$$p_{capture} \simeq e^{-1/2(v'_{nL})^2/v_c^2} \tag{61a}$$

where

$$v_c = 2 \, v_{max}/2.35 \quad . \tag{61b}$$

This approximation allows us to explicitly carry out the integration of eq. (60). Thus, we can write the source density $\vec{S}_{u.c.}$ for Ultra-Cold Neutrons

as

$$\vec{S}_{u.c.} = \int e^{-1/2(v'^2_{nL}/v_c^2)} \vec{S}\, d^3\vec{v}'_{nL} \quad . \tag{62}$$

The magnitude of this current density can be analytically evaluated. The result is

$$S_{u.c.} = r\gamma_o n_p v_R^o I_x I_y I_z \tag{63}$$

where

$$I_j = \sqrt{\frac{2\pi}{A_j}}\, e^{-1/2[C_j - B_j^2/4A_j]} \quad (j = x,y,\text{or } z). \tag{64}$$

The dependence of $S_{u.c.}$ on x,y, and t is contained in the functions A_j, B_j, C_j. The functions are displayed in Table III. (For convenience we have defined $\tau = \tau_g/2.35$). Note that the time t appears explicitly in these expressions and also implicitly in $\Delta V'_x$, $\Delta V'_y$, $\Delta V'_z$ (see eq. (48)). Note also that we have suppressed the additional subscripts nL on the velocities. The results depend upon the mosaic and collimation parameters n_x, n_y, α_x, and α_y through the definitions of W_x, W_y, and W_z (eqs. 9, 10, 11), and explicitly on the pulse width τ and the maximum velocity v_{max} $(= \frac{2.35}{2} v_c)$.

Based on the instrumental parameters given in Table II, we have performed numerical calculations of $S_{u.c.}$ given by eq. (63). We find that $S_{u.c.}$ is only a weak function of the y-coordinate on the crystal face. The dependence of $S_{u.c.}$ on the x-coordinate at various times t is shown in Fig.5. As the rotor turns and brings the crystal into the beam, Ultra-Cold Neutrons are first generated from the left-hand side of the crystal ($x > 0$, see Fig. 2). At $t = 0$, the crystal is at the beam center line, and the emission of Ultra-Cold Neutrons is symmetric in x across the crystal face. As the rotor continues to turn ($t > 0$) the right-hand side ($x < 0$) becomes the primary source of Ultra-Cold Neutron production. For $|t| >> \tau$, the edges of the collimator

will shadow a part of the crystal. For a collimator of width W (at the crystal), the x-coordinate of the collimator edges projected onto the crystal is given by

$$x_L = \frac{W}{2} - R\theta \sin\beta \qquad (65a)$$

on the left, and

$$x_R = -\frac{W}{2} - R\theta \sin\beta \qquad (65b)$$

on the right. At $t = -180\mu s$, $x_L = 6.39$ cm, and $x_R = -2.47$ cm. At $t = +180$ μs, $x_L = 2.47$ cm and $x_R = -6.39$ cm. Since the Ultra-Cold Neutron production is small outside this time frame (-180 μs $< t <$ 180 μs) we conclude that the effects of this collimator shadowing consideration are minimal for a crystal of width $\lesssim$ 5 cm. For a crystal of width 2 cm, we have integrated the curves of Fig. 5 over the crystal face to obtain the total production rate of Ultra-Cold Neutrons. We display the results of this calculation as a function of the rotor angle $\theta = \omega t$ in Fig. 6. If we integrate this curve over the time t, we have the total Ultra-Cold Neutron production per pulse; the result is

$$\text{Ultra-Cold Neutrons/pulse} = 6{,}000 \quad \text{(IPNS-I)} . \qquad (66a)$$

This number should be compared with the total number of neutrons in the velocity space volume A (Fig. 3) integrated over time. This is the maximum number of neutrons coming from the source which could potentially be Doppler-shifted to Ultra-Cold velocities; it is approximately

$$N_{max} = n_p \frac{4}{3} \pi v_{max} v^{\circ}_{nL} \tau A = 76{,}000. \quad \text{(IPNS-I)} . \qquad (66b)$$

Here, A (= 5 cm X 2 cm) is the area of the crystal. Thus, the overall efficiency is about 8%. The main sources of the inefficiency are that the mosaic spread of the crystal (3°) is too small and the collimation (α_x,α_y) is also too small. Using a beam guide and a 6° mosaic crystal, we expect

that this efficiency could be improved by as much as a factor of 5. (It is possible to artificially increase the mosaic spread in one direction by using an assembly of thinner crystals with wedges between. For example, refer to the Appendix.)

IV. MONTE CARLO COMPUTER SIMULATION

In this section we describe a more exact numerical calculation of the Bragg reflection process to produce UCN and their subsequent collection in a neutron bottle. The calculation was carried out for the specific arrangement shown in Fig. 1 and the parameters in Table II, and was checked using the analytic formulae developed in the previous section.

A. General Discussion

In order to avoid many of the approximations used above to describe the details of the Bragg scattering process, the computer simulation was carried out at a microscopic level. The crystal was pictured as a collection of small mosaic blocks Gaussianly distributed in angle about the nominal normal to the crystal face and each capable of reflecting neutrons with 100% probability if the Bragg angle were satisfied to within the Darwin width (refer to the Appendix). The crystal was assumed to have finite dimensions, and to have a mosaic angular spread η_x in the x-direction and η_y in the y-direction. Finally, once a neutron was reflected its depth of penetration into the crystal was noted and the neutron was permitted to undergo multiple reflections. As the flight path within the crystal could be fairly long, the absorption probability was also considered.

The Monte Carlo simulation begins with neutrons at the source, allowing them to propagate through the beam tube resulting in a time-broadening of the pulse at the crystal due to the spread in incident velocities. The rotor angle changed with time according to $\theta = \omega t + \alpha$ with the phase of the rotor α being a variable. It was set externally by optimizing the number of neutrons reflected into the sphere in velocity space of radius v_{max}. Neutron trajectories after reflection were checked to determine if

the neutron arrived at the bottle entrance during the time the shutter was open. The phase angle between the shutter and the rotor was also a variable and set externally by optimizing the total number of neutrons collected in the bottle per pulse.

B. Scattering Process Simulation

For a given incident neutron in the crystal frame, with a velocity vector $\vec{v}_{nR}$ oriented with direction cosines $\cos\xi_x$ and $\cos\xi_y$, the probability of finding a mosaic block satisfying Bragg condition (5) is[35]

$$P(x,y) = \frac{1}{2\pi\eta_x\eta_y} \exp\left[- \frac{1}{2} \left(\frac{\xi_x^2}{\eta_x^2} + \frac{\xi_y^2}{\eta_y^2} \right) \right]. \qquad (67)$$

The probability of scattering at a point in the crystal at distances between ℓ and $\ell + d\ell$ along a trajectory is given by

$$p_\ell d\ell = e^{-\ell\Sigma s} \Sigma_s d\ell \qquad (68)$$

where Σ_s is the probability of scattering per unit length which can be calculated using (67)

$$\Sigma_s = QP(x,y) \qquad (69)$$

For 17.3 Å neutrons and a Bragg angle of 61.2°, Q is 7.9 cm^{-1} for the synthetic mica crystal described in the Appendix.[36] This yields an average penetration depth of 0.0162 cm for a crystal with a 3° mosaic spread. The average distance traveled by a neutron inside the crystal, including multiple rescattering, was found to be about 1/3 millimeter.

It was assumed that the crystal did not rotate during the time period (including all rescatters) that the neutron spent inside the crystal. This last approximation was reasonable as the probability for scattering changed by only 10% for a rotor angular change experienced in a 10^{-4} sec. time period.

For neutrons moving at 225 m/s in the crystal frame this would correspond to a total flight path of 2 cm inside the crystal, far from the average flight path indicated above.

The Monte Carlo results were compared with a published analytic calculation of a multiple scattering problem[37] and the results are shown in Fig. 7 for single and triple reflections. The explanation of the coordinate h is also shown in the figure. The curves are in good agreement. These results lend confidence that the program was adequately simulating the details of the scattering process in the crystal.

C. Normalization

Neutrons were randomly generated across the surface of the source shown in Fig. 1 within some velocity volume Δv_x, Δv_y, Δv_z around a nominal v°_{zL} setting of 395 m/s. The time variation of the pulse at the source was assumed to be Gaussian in a manner which was used to obtain equation (55). Thus the phase space density n_s at the source was assumed to be

$$n_s(x,y,z,v_x,v_y,v_z,t) = n_p \, e^{-t^2/2\tau_g^2} \quad . \tag{70}$$

where n_p is the peak phase space density and $\tau_g = \tau/2.35$ (as in the previous section). As the average $v_{nL} \approx v^\circ_{zL}$ the overall normalization used in the Monte Carlo calculation for each generated neutron was

$$\text{Norm} = n_p \Delta v_x \Delta v_y \Delta v_z \pi r_s^2 v_{zL} \tau_g / N_G \tag{71}$$

where r_s was the source radius and N_G the number of neutrons generated in the program.

D. Results

In Fig. 6 we make a comparison between the predicted Monte Carlo production rate of Ultra-Cold Neutrons S as a function of rotor angle and the analytic results presented in the previous section. The shapes of the curves agree but the computer simulation is 14% higher and predicts the total UCN production rate of

$$\text{Ultra-Cold Neutrons/pulse} = 7{,}000 \ . \qquad (72)$$

The reason for the disagreement is due to the approximations made in the analytic calculation where we ignored the time variation of the distance from the source to the crystal, and we approximated the collimation and $P_{capture}$ (eq. 61) by Gaussians.

Also shown in Fig. 6 is the number of neutrons collected in the bottle (cross hatched region). This number per pulse is

$$N_p = \text{Ultra-Cold Neutrons collected/pulse} = 1{,}300 \ . \qquad (73)$$

Comparing (72) and (73) shows that the collection efficiency is about 19%. This is the efficiency expected as the solid angle subtended by the bottle opening is ~ 0.4 of a sphere while the finite time the door remains open (3 msec) allows only 50% of the neutrons heading toward the bottle to enter. It should be noted that the collection efficiency does not effect the final density of stored neutrons as this depends on the flux of UCN coming off the crystal which remains constant for many milliseconds until the reflected cloud of UCN diffuses away. However, the filling time is effected by the collection rate.

In Fig. 8 the velocity distribution of neutrons in the bottle is shown for $v_{MAX} = 7$ m/s. Their mean speed is $\bar{v} = 4.4$ m/s. The deficiency of

neutrons above 6 m/s is caused by a smaller velocity space volume being reflected than can be captured in the bottle. This mismatch was noted earlier in the previous section and can be corrected by a larger mosaic spread and the use of a guide tube in the beam.

For a given N_p rate, the final density ρ_{MAX} to which the bottle can be filled depends on the loss rate out of the bottle, i.e., the loss of neutrons out of the door when the shutter is open plus the losses contributing to the overall bottle storage time, τ_B. This storage time is characterized by an exponential decay e^{-t/τ_B} . As noted earlier τ_B should be 1000 s optimally, but has been measured to be much less. Therefore, we present the values for ρ_{MAX} as a function of τ_B.

The loss through the shutter is computed using gas kinetics assuming that the UCN behave as an ideal gas inside the bottle. From elementary statistical physics[38] the loss rate per unit time through a shutter with an area A is

$$\nu = \frac{1}{4} \rho A \bar{v} \qquad (74)$$

where ρ is the neutron density in the bottle at time t and $\bar{v}$ is the mean speed of the neutrons in the bottle.

For τ_B, N_p and equation (72), with $\bar{v}$ taken from Fig. 8; ρ_{MAX} was estimated for IPNS and plotted in Fig. 9. The density approaches saturation for $\tau_T \sim 300$s and is

$$\rho_{MAX} = 120 \text{ n/cm}^3 \quad . \qquad (75)$$

This does not imply that τ_B values larger than 300s are not desirable. This is clearly dependent on experimental details and can be very important in an EDM measurement, where the sensitivity varies inversely to τ.

In Table IV the asymptotic densities and filling times are listed. For a 10 liter bottle these times are generally on the order of minutes or about 6000 pulses. The total number of stored neutrons N_o is predicted to be 1.2×10^6.

In the above calculation we have assumed that the crystal reflectivity is 100% though it may be considerably less (refer to the Appendix). There will also be absorption losses in the crystal holder and losses of neutrons due to the loose fit of the shutter over the bottle mouth. The sum of these effects could reduce the stored density by a factor of 2 or 3.

V. CONCLUSIONS

The two independent calculations presented above are in good agreement for the production of Ultra-Cold Neutrons using Doppler-shifting at the Intense Pulsed Neutron Source. Given the range of uncertainties the density of stored neutrons is predicted to be between 40 and 120 n/cm^3. Using these numbers to estimate the sensitivity in a proposed EDM experiment,[4] we conclude that a measurement with a statistical uncertainty near 10^{-27} e-cm can be performed. However, a practical experiment also requires various systemmatic effects to be reduced in order to achieve this sensitivity.[4,8,14,28]

The Doppler-shifting method described in this paper is well matched to a pulsed source as the Bragg reflecting crystal is only effective over a short period of time. However, there is an advantage in using this method to produce UCN even at a steady state source in that the primary transport velocity is much higher ($\sim$ 400 m/s)

and the UCN are produced closer to the experimental area. The absorption losses of UCN that can be sèvere in a reactor beam are much reduced.

There are a number of inefficiencies that have been identified in the Bragg scattering off a moving crystal. The total efficiency of scattering into a sphere of radius v_{max} was found to be $\sim$ 10%. Using a guide tube in the incident beam and a broader mosaic spread could yield a factor of 5 increase in neutron density. The remaining inefficiency is due to the velocity differential produced across the crystal by the differential in radius on the rotor and the time slewing of the incident pulse. Also, a Bragg angle of 61.2° is not the optimal value for the maximum efficiency. Building a larger rotor and moving nearer the source would help reduce these losses. However, such modifications are limited by practical considerations.

The bottle collection efficiency was found to be $\sim$ 20% of the UCN produced. As noted in the previous section this does not effect the final density in the bottle, however the filling time is increased. Using reflectors placed around the rotor more of the solid angle can be reflected toward the bottle opening. In this manner a factor of 2 shortening of the filling time may result.

The shutter mechanism insures that the bottle is filled as if by an incident beam at the peak flux of the source. Pulsed neutron sources can be expected to improve their peak intensities in years to come and a corresponding increase in density of stored UCN can be expected. On the other hand, it is doubtful that much higher thermal fluxes from steady state reactors are possible due to heat transfer limits and construction and operating costs.

There are a number of additional advantages working at a pulsed source over a steady state reactor. Background levels are in general reduced as the time-average flux is much lower. As the heat load and radiation damage are smaller in pulsed sources, better cold moderators may be possible to construct and operate than have been possible for reactors resulting in an increase in flux at the longer wavelengths needed for the Doppler-shifter.

ACKNOWLEDGEMENTS

The authors wish to express their gratitude to the staff at the National Bureau of Standards reactor for permitting us to make measurements on our crystal assembly. We also wish to thank Gene Hardekopf who helped obtain these measurements. This work has been supported in part by the U.S. Department of Energy. One of the authors (S.A.W.) wishes to acknowledge support in part by the Physics Division, NSF through Grant No. NSF-PHY 7608960, and another author (J.W.L.) through NSF Grant No. DMR-76-81185.

APPENDIX

Details of Bragg Scattering by a Crystal

Bragg scattering off a mosaic crystal can be characterized by two parameters: The peak reflectivity γ_o and the effective, in-plane mosaic width, η_{eff} [rocking curve width]. If we approximate the rocking curve by a Gaussian, then the reflectivity is

$$\gamma(\Delta) = \gamma_o e^{-\Delta^2/2\eta_{eff}^2}, \tag{A1}$$

where Δ is the orientation of the crystal with respect to the nominal Bragg setting. In Darwin's mosaic crystal model, the probability per unit path length for a neutron to be Bragg reflected within the crystal is

$$\Sigma_s(\Delta) = QW(\Delta), \tag{A2}$$

where $W(\Delta)$ is the distribution function describing the orientation of mosaic grains, and Q is the crystallographic quantity:

$$Q = \frac{\lambda^3 |F|^2}{V_{cell}^2 \sin 2\theta_B} \tag{A3}$$

V_{cell} is the volume of the unit cell, θ_B is the Bragg angle, λ is the neutron wavelength, and F is the structure factor. If we assume that the mosaic grains are distributed in a Gaussian way, then

$$W(\Delta) = \frac{1}{\sqrt{2\pi}\,\eta_H} e^{-\Delta^2/2\eta_H^2}. \tag{A4}$$

For synthetic mica (Thermica)[36], having the chemical formula $KMg_3AlSi_3O_{12}F_2$, the d-spacing is 9.963 Å, the density is 2.67 gm/cm^3, and

$$Q = 7.9\ cm^{-1}, \tag{A5}$$

for a wavelength of 17.3 Å ($\theta_B = 60°$). The absorption length for this crystal is calculated to be 79 cm. For a crystal of thickness T, placed

in the symmetric Bragg reflection geometry, this model gives a reflectivity

$$\gamma(\Delta) = \frac{QW(\Delta)T/\sin\theta_B}{1 + QW(\Delta)T/\sin\theta_B} \quad , \qquad \text{(A6)}$$

for the case of zero absorption. Thus, experimentally, one approximates this expression by eq.(A1).

"Rocking Curve" measurements were made on samples of Thermica placed in a 2.24Å wavelength neutron beam at the National Bureau of Standards (NBS) reactor. For a 0.01 inch thickness the "rocking curve" for a 1" X 1" piece is shown in Fig. A1. The measured FWHM after unfolding the beam divergence was found to be 0.27° and the peak reflectivity was 4.2%. Thinner pieces yielded mosaic spreads from 1/4° to 1/2° but lower reflectivities.

As indicated in the text a crystal with a small mosaic in y and a 6.0° mosaic in x would best match the beam arrangement described in Fig.1 and Table II. A composite crystal was fabricated with thin (0.010 inch) pieces of Thermica sandwiched between thin (0.005 inch) wedges of aluminum arranged to give a 6° spread in angle in the x-direction and no additional spread in y. The assembly composed of 15 such sub units was tested in the NBS beam. The results are shown in Fig. A2 and show that the mosaic spreads are different, the spread being about 6° (FWHM) in the x-direction and about 1.25° in the y-direction. The peak reflectivity is ∿5% at 2.24 Å.

The peak reflectivity at 17.3Å will be much higher. Using eq. (A6), we can estimate this increase by writing

$$\frac{QW(0)T}{\sin\theta_B} = \frac{c\lambda^3}{\sin\theta_B \sin 2\theta_B} \quad . \qquad \text{(A6)}$$

At $\lambda = 2.24\text{Å}$, $\theta_B = 6.45°$. For the assembly of crystals $\gamma_o = 0.05$ at this wavelength; this requires the constant c to be

$$c = 1.11 \times 10^{-4}, \tag{A7}$$

where λ has been expressed in Å. At 17.3Å ($\theta_B = 60°$), we then have

$$\frac{QW(0)T}{\sin\theta_B} = \frac{1.11 \times 10^{-4} (17.3)^3}{\sin 60° \sin 120°} = 0.76. \tag{A8}$$

Thus, according to (A6)

$$\gamma(0) = \gamma_o = 0.43. \tag{A9}$$

A transmission measurement was performed using 18.7 Å neutrons incident on a Thermica crystal assembly similar to that described above. The reflectivity was found to be 47% for a 1/2-inch total thickness of Thermica. This result implies that the quantity γ_o in equations 59 and 63 may be nearer a value of 0.5 rather than 1.0 as assumed in the calculations, in the text.

REFERENCES

[1]F.L. Shapiro, Soviet Phys. Usp. 11, 345 (1968).

[2]A. Steyerl, Nucl. Instr. and Methods 101, 295 (1972).

[3]A. Steyerl, Nucl. Instr. and Methods 125, 461 (1975).

[4]T. Dombeck, Preprint No. 78-074, Univ. of Maryland (1977).

[5]P. Ageron et al., Preprint IAEA-M-219/58, ILL Grenoble (1977).

[6]A. Steyerl, Springer Tracts on Modern Physics 80, 57 (1977).

[7]R. Golub and J.M. Pendlebury, Contemp. Phys. 13, 519 (1972).

[8]N.F. Ramsey, in Atomic Physics, eds. R. Marrus, M. Prior, and H. Shugart, (Premium Press, New York, 1977).

[9]C.G. Shull and N.S. Gingrich, Journal of Applied Physics 35, 678 (1963).

[10]B. Buras and J. Kjems, Nucl. Inst. and Methods 106, 461 (1973).

[11]S. Steenstrup and B. Buras, Nucl. Instr. and Methods 154, 549 (1978).

[12]J. Carpenter, D.L. Price, and J.J. Swanson, "IPNS. A National Facility for Condensed Matter Research," ANL-78-88, Argonne National Laboratory (1978); see also J.M. Carpenter, Nucl. Instr. and Methods 145, 91 (1977).

[13]J.M. Christensen et al., Phys. Rev. Lett. 13, 138 (1964).

[14]I.S. Altarev et al., "Search for an Electric Dipole Moment of the Neutron by Means of the Ultra-Cold Neutrons, " Preprint no. 430, Konstantinov Institute of Nuclear Physics, Leningrad, USSR (1978).

[15]W.B. Dress et al., Phys. Rev. D15, 9 (1977).

[16]N.G. Deshpande and E. Ma, Phys. Rev. D16, 1513 (1977).

[17]S. Weinberg, Phys. Rev. Lett. 37, 657 (1976).

[18]J. Pati, Tech. Rep. No. 78-073, Univ. of Maryland (1978).

[19]B.W. Lee, Phys. Rev. D15, 3394 (1977).

[20]L. Wolfenstein, Nucl. Phys. B77, 375 (1974).

[21]P. Sikivie, Phys. Lett. 65B, 141 (1976).

[22]N.F. Ramsey, Molecular Beams (Oxford Univ. Press, Oxford, England, 1956).

[23]L.V. Groshev et al., Phys. Lett. 34B, 293 (1971).

[24]L.V. Groshev et al., Preprint P3-7282, JINR, Dubna, USSR (1973).

[25]F. Shapiro, Preprint P3-7135, JINR, Dubna, USSR (1973).

[26]A. Steyerl and W. Trüsteadt, Z. Physik 267, 379 (1974).

[27]L.V. Groshev et al., Preprint P3-9534, JINR, Dubna, USSR (1976).

[28]F. Smith et al., "Search for the Neutron Electric Dipole Moment Using Bottled Neutrons", Research Proposal, ILL, Grenoble (1974).

[29]K. Inoue, Y. Kiyanagi, and H. Konno, J. Nucl. Sci. Technol. 14, 195 (1977).

[30]C.G. Shull, K.R. Morash, and J.G. Rogers, Acta Cryst. A24, 160 (1968).

[31]B. Buras, T. Giebultowicz, W. Minor, and A. Rajca, Nucl. Instr. and Methods 70, 13 (1970).

[32]B. Buras and T. Giebultowicz, Acta Cryst. A28, 151 (1972).

[33]D. Bally, E. Tarina, and N. Papa, Nucl. Instr. and Methods 127, 547 (1975).

[34]S.A. Werner and R. Pynn, J. Appl. Phys. 42, 4736 (1971).

[35]G.E. Bacon, Neutron Diffraction (3rd Ed., Oxford, Clarendon Press, 1975).

[36]A.N. Goland and J.H. Sondericker, Rev. Sci. Instr. 30, 269 (1959).

[37]S.A. Werner and A. Arrott, Phys. Rev. 140, A675 (1965).

[38]C. Kittel, Elementary Statistical Physics (John Wiley and Sons, Inc., N.Y., 1958).

TABLE I. Limiting Velocities for Total Internal Reflection of Ultra-Cold Neutrons

Material	v_{MAX}(m/s)[a]
Be	6.9
BeO	6.9
Fe[b]	8.2 4.15
Ni[b]	7.2 6.2
C	5.8
Cu	5.6
Al	3.22

[a] $v_{MAX} = \frac{h}{m}\sqrt{\frac{Na}{\pi}}$, where m is the neutron mass, N is the density of scattering centers, a is the coherent scattering length and h is Planck's constant.

[b] Ferromagnetic materials have two limiting velocities depending on the neutron spin direction relative to the magnetic field.

TABLE II. Design Parameters For the Doppler Shifter to Be Used at the Argonne Laboratory Intense Pulsed Neutron Source

A.	Source	
	Pulse rate	30 Hz
	Beam Velocity	395 m/s
	Phase Space Density	0.66 $n/cm^3 - (m/s)^3$
	Pulse Width (FWHM)	200 μs
	Beam Diameter	10 cm
	Distance Source to Crystal	480 cm
B.	Rotor and Crystal	
	Radius	120.2 cm
	Bragg Angle	61.2 degrees
	d-spacing	9.96Å (Thermica crystal)
	Mosaic Spread (η_x)	1/2 degree
	Mosaic spread (η_y)	3 degrees
	Crystal Dimensions	5 cm x 2 cm
	Crystal Thickness	0.4 cm
	Shutter Time Interval	3 ms
C.	Bottle	
	Bottle Opening	5 cm x 6 cm
	v_{MAX} (Beryllium)	7 m/s
	Volume	10 ℓ

TABLE III. Expressions for the Functions of A_j, B_j, C_j

	A_j	B_j	C_j
x	$\left(\frac{1}{v_c^2} + \frac{1}{W_x^2}\right)$	$-\frac{2\Delta V'_x}{W_x^2}$	$\frac{\Delta V'^2_x}{W_x^2}$
y	$\left(\frac{1}{v_c^2} + \frac{1}{W_y^2}\right)$	$-\frac{2\Delta V'_y}{W_y^2}$	$\frac{\Delta V'^2_y}{W_y^2}$
z	$\left(\frac{1}{v_c^2} + \frac{1}{W_z^2} + \frac{L_o^2}{(v^o_{nL})^4 \tau_g^2}\right)$	$\left(\frac{L_o t}{(v^o_{nL})^2 \tau_g^2} - \frac{2\Delta V'_z}{W_z^2}\right)$	$\left(\frac{\Delta V'^2_z}{W_z^2} + \frac{t^2}{\tau_g^2}\right)$

TABLE IV. Bottle Filling Rates and Stored Densities[a]

v_{MAX}(m/s)	ϵ_{DS}[b]	N_p[c]	ρ_{MAX}(n/cm^3)[d]	τ_F(s)[e]
5	0.11	580	70	230
7	0.10	1300	120	200

[a]Assumes a 10ℓ bottle with a 30 cm^2 opening.

[b]Assumes a 5 cm x 2 cm thermica crystal with $\eta_y = 3°$, $\eta_x = 1/2°$, $\theta_B = 61.2°$ and shutter speed of 3 ms. This is the efficiency of scattering into a sphere in velocity space of radius v_{MAX}.

[c]Number of neutrons per pulse entering the bottle.

[d]Asymptotic density of stored neutrons.

[e]Filling time to arrive at the asymptotic density.

FIGURE CAPTIONS

Fig. 1. An overall schematic diagram of the apparatus to be used to search for the neutron EDM at the pulsed sources at Argonne National Laboratory. The Doppler-shifter (rotor) is currently being tested at the ZING-P' source. It is 2.4m in diameter and turns at 30 Hz.

Fig. 2. This figure defines the symbols used in the text to describe the Doppler-shifter as viewed in the laboratory (A) and as viewed in velocity space (B). The velocity vector $\vec{v}_R$ of the moving crystal makes an angle β with the beam center line $(\hat{z})$ when the center of the crystal passes the beam center. The nominal Bragg angle θ_B is related to β by $\theta_B = \pi/2-\beta$.

Fig. 3. This diagram shows the velocity space volumes effective in the Doppler-shifting process, and how the neutron distributions as viewed in the laboratory (L) and in the moving (R) frames are related. The dimensions $\overline{W}_z = 2.35\ W_z$ and $\overline{W}_x = 2.35\ W_x$ are given by eqs. (10) and (9) respectively. The third dimension $\overline{W}_y = 2.35\ W_y$ of volumes B' and C is given by eq. (11).

Fig. 4. This figure shows the overlap (shaded region) of the Doppler shifted neutrons with a sphere of radius v_{max} in the $v'_{xL} - v'_{zL}$ plane. The top part (A) of the figure is for the point x = 0, y = 0 on the crystal face. The bottom part (B) of the figure is

for a point x = 2 cm, y = 0. The machine parameters used to construct these figures are given in Table II.

Fig. 5. This figure shows the Ultra-Cold Neutron source intensity $S_{u.c.}$ at various times t as a function of position x across the crystal face. The parameters of Table II were used as input data.

Fig. 6. The total Ultra-Cold Neutron production rate, which is the integration of the curves of Fig. 5 over the crystal area, is plotted here as a function of the rotor angle $\theta = \omega t$ (solid curve). The y-dimension of the crystal was taken to be 5 cm, while the x-dimension was 2 cm. Also shown are the results for the Monte Carlo simulation (dashed curve). The cross hatched region is the number of neutrons arriving in the bottle. Parameter values were set using Table II. The crystal reflectivity γ_o was taken to be 100%.

Fig. 7. This figure shows a comparison between the Monte Carlo simulation of multiple reflections within the crystal and the analytic calculation taken from Ref. 37. The slight differences observed are due to the finite crystal size taken in the Monte Carlo simulation whereas the calculation assumed a semi-infinite crystal.

Fig. 8. The velocity distribution of neutrons in the bottle is plotted. The average velocity is 4.4 m/s for v_{MAX} = 7 m/s. The parameters in Table II were used as input to the Monte Carlo program. dN/dv is the number of neutrons per unit velocity increment.

Fig. 9. The expected asymptotic storage density of neutrons in the bottle after many pulses is plotted versus the bottle storage time, τ_B. The parameters input for the Monte Carlo program were set using Table II. The crystal reflectivity was taken to be 100%.

Fig.A1. This histogram is the "rocking curve" for a piece of Thermica described in the appendix. The measurements were made at the National Bureau of Standards reactor in a 2.24 Å neutron beam. The sample dimensions were 1" X 1" and 0.01 inch in thickness.

Fig.A2. The two histograms presented here are the "rocking curves" for an assembly of thin Thermica crystals separated by wedges of aluminum as described in the appendix. There were 15 such sub-units having one 0.01 inch piece of mica sandwiched between 0.005" pieces of aluminum. The resulting curves indicate a larger mosaic width in x than in y as desired.

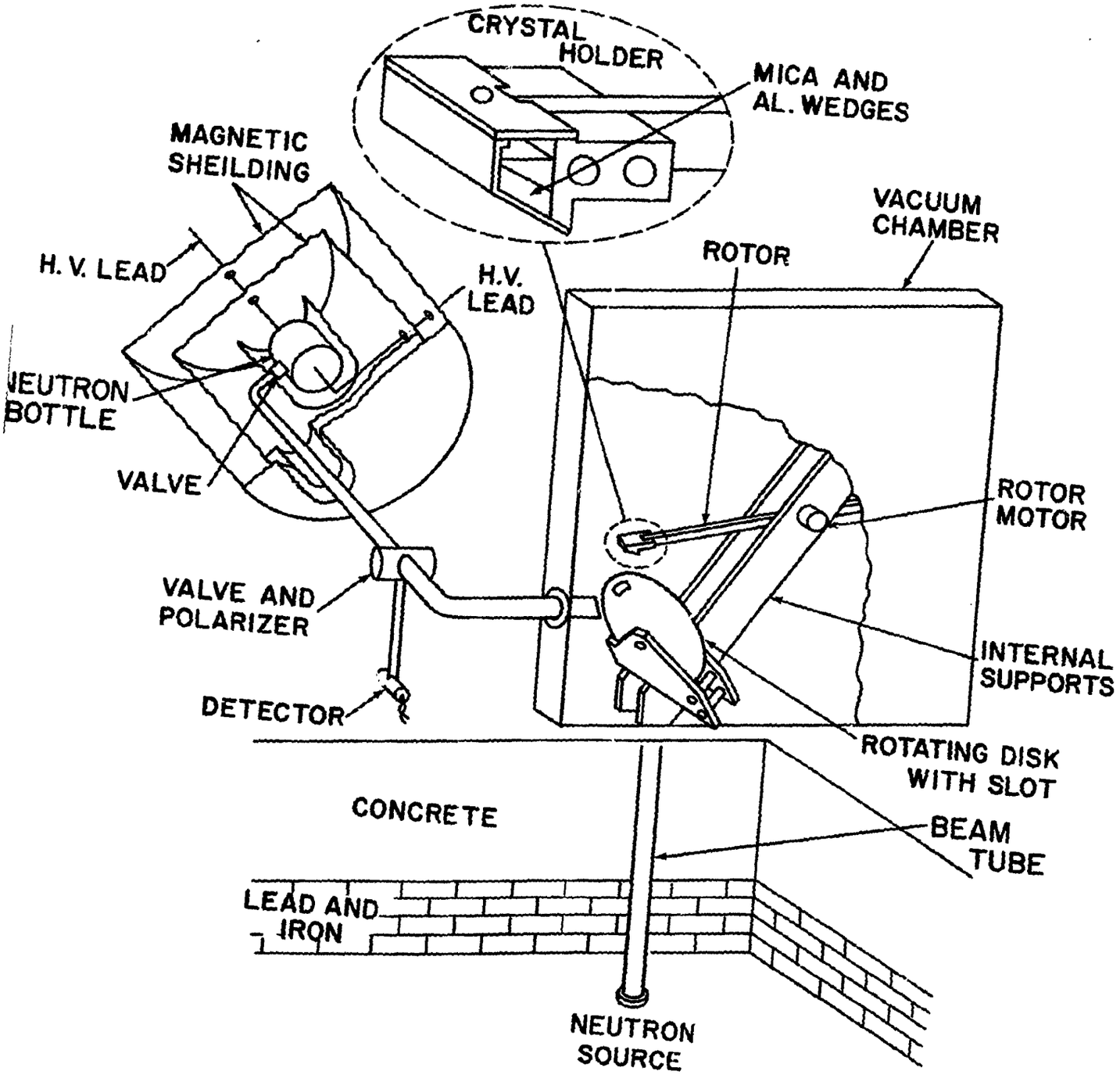
CRYSTAL HOLDER
MICA AND AL. WEDGES
MAGNETIC SHEILDING
VACUUM CHAMBER
H. V. LEAD
ROTOR
H.V. LEAD
NEUTRON BOTTLE
VALVE
ROTOR MOTOR
VALVE AND POLARIZER
INTERNAL SUPPORTS
DETECTOR
ROTATING DISK WITH SLOT
CONCRETE
BEAM TUBE
LEAD AND IRON
NEUTRON SOURCE

Fig. 1.

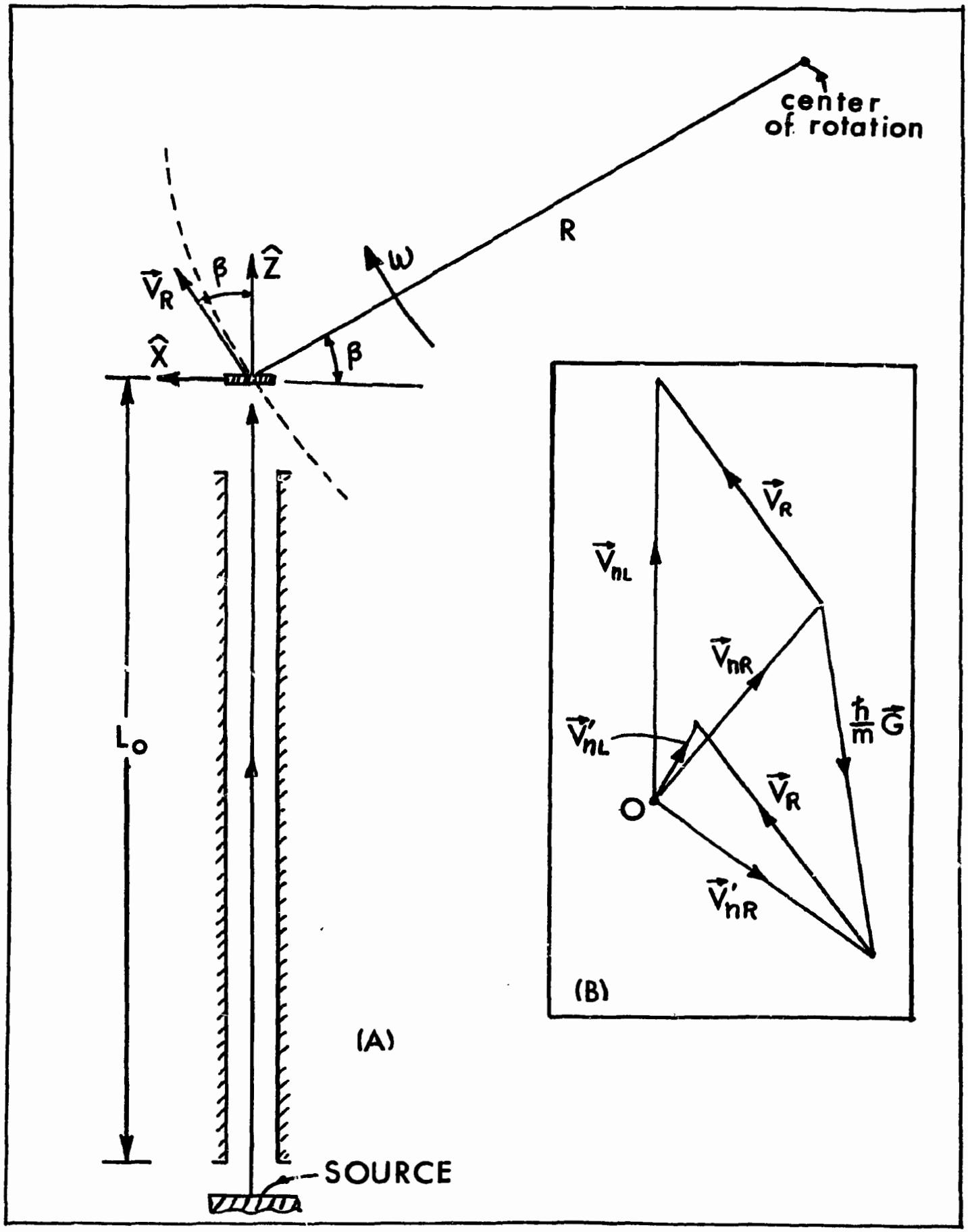
center
of rotation
R
ω
β
$\hat{Z}$
$\vec{V}_R$
$\hat{X}$
β
L_o
SOURCE
(A)
$\vec{V}_R$
$\vec{V}_{nL}$
$\vec{V}_{nR}$
$\frac{h}{m}\vec{G}$
$\vec{V}'_{nL}$
O
$\vec{V}_R$
$\vec{V}'_{nR}$
(B)

Fig. 2.

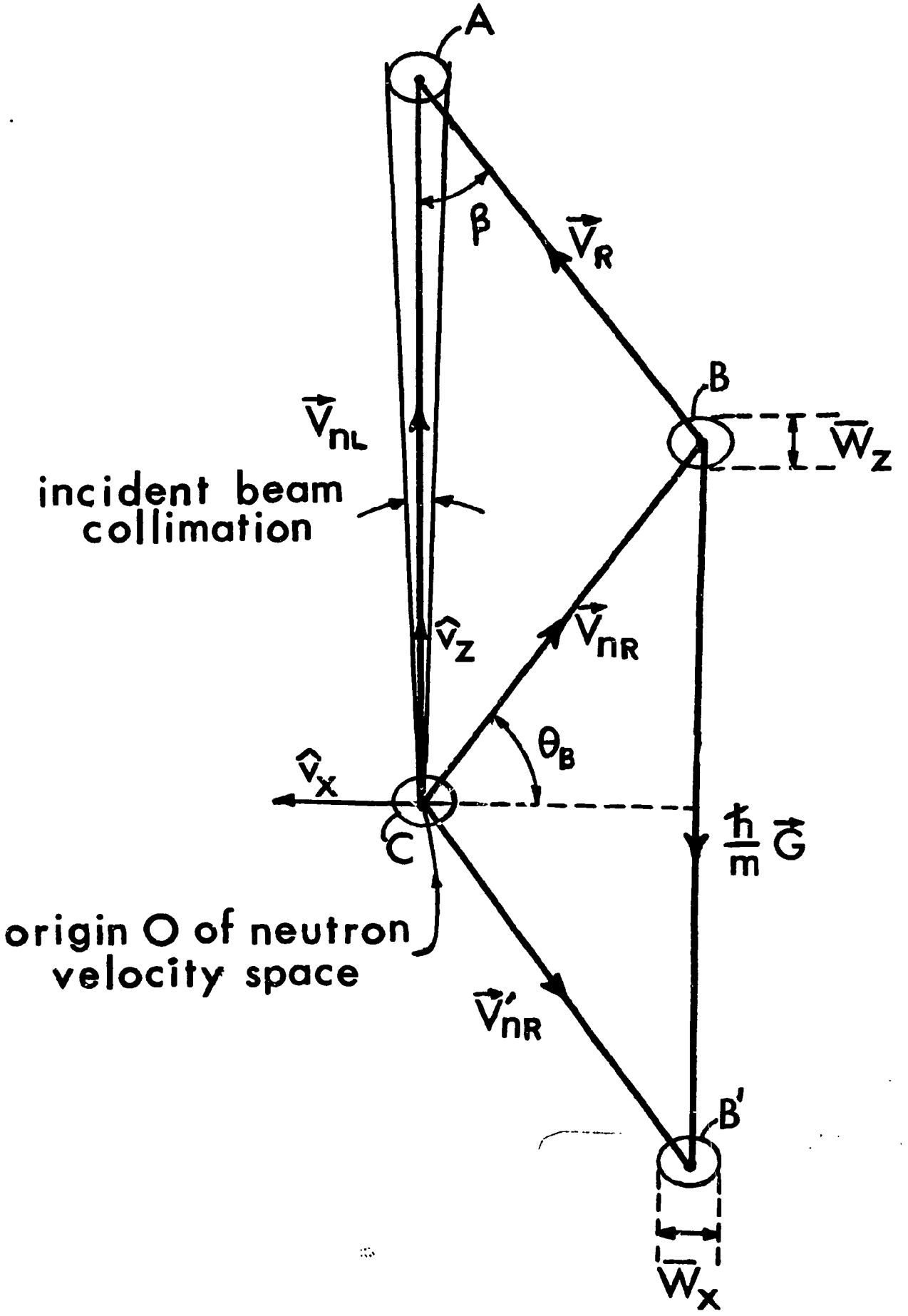
A
β
$\vec{V}_R$
B
$\vec{V}_{nL}$
$\bar{W}_z$
incident beam
collimation
$\hat{v}_z$
$\vec{V}_{nR}$
θ_B
$\hat{v}_x$
C
$\frac{\hbar}{m}\vec{G}$
origin O of neutron
velocity space
$\vec{V}'_{nR}$
B'
$\bar{W}_x$

Fig. 3.

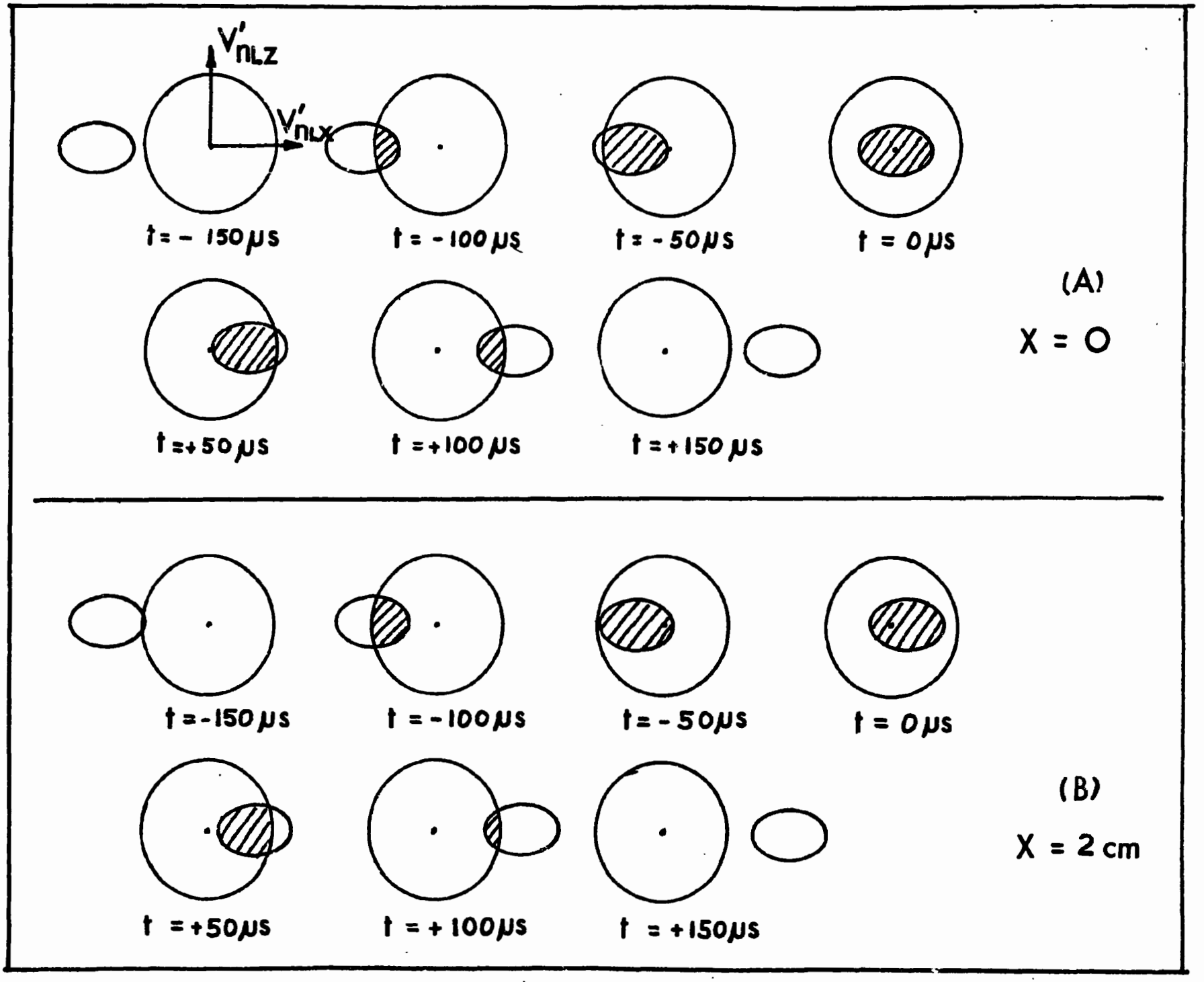
V'_{nLz}
V'_{nLx}
t = - 150 μs
t = - 100 μs
t = - 50 μs
t = 0 μs
t = + 50 μs
t = + 100 μs
t = + 150 μs
(A)
X = O
t = - 150 μs
t = - 100 μs
t = - 50 μs
t = 0 μs
t = + 50 μs
t = + 100 μs
t = + 150 μs
(B)
X = 2 cm

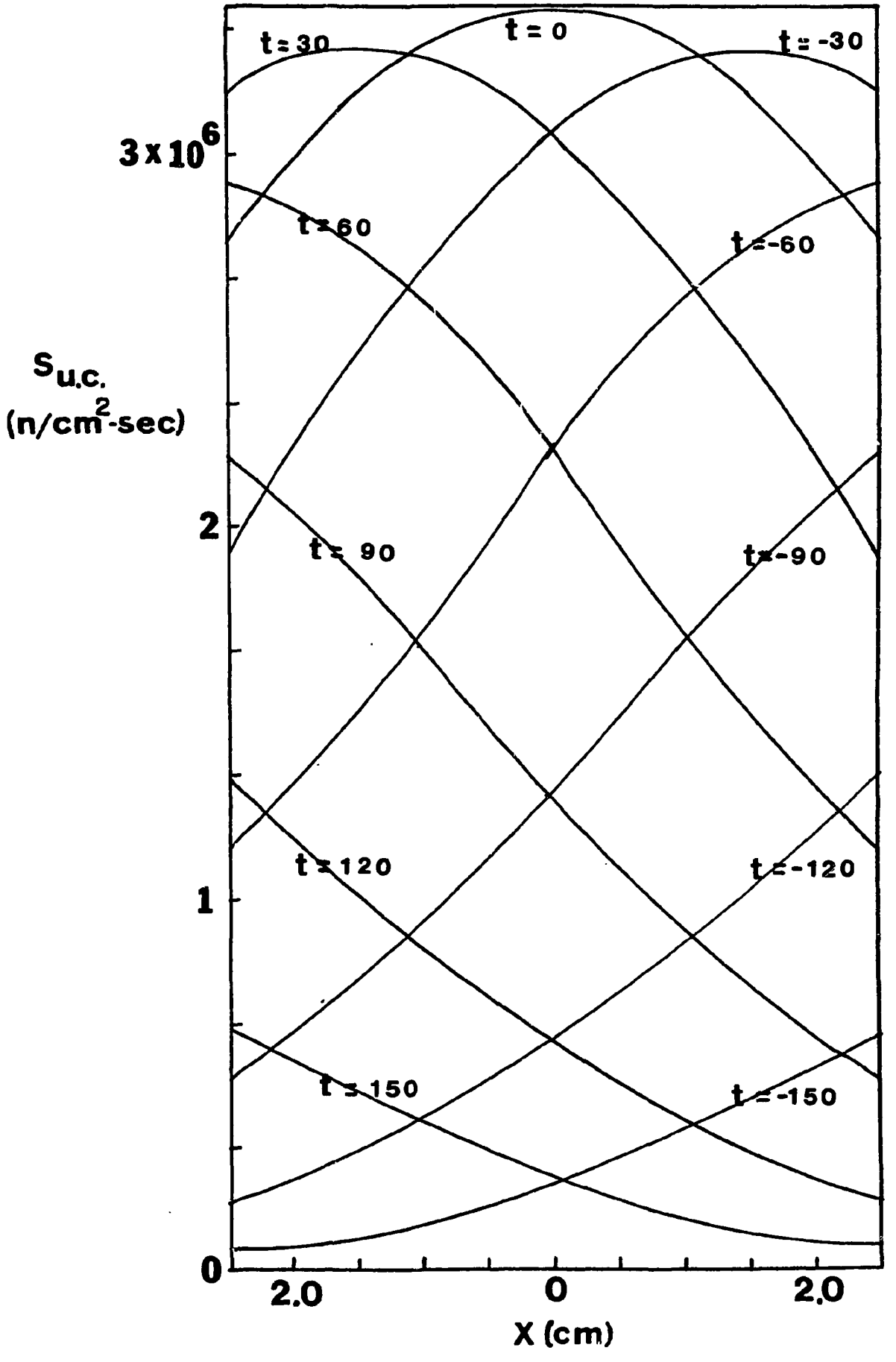
t = 30
t = 0
t = -30
3 x 10^6
t = 60
t = -60
S u.c.
(n/cm^2-sec)
2
t = 90
t = -90
t = 120
t = -120
1
t = 150
t = -150
0
2.0
0
2.0
X (cm)

Fig. 5

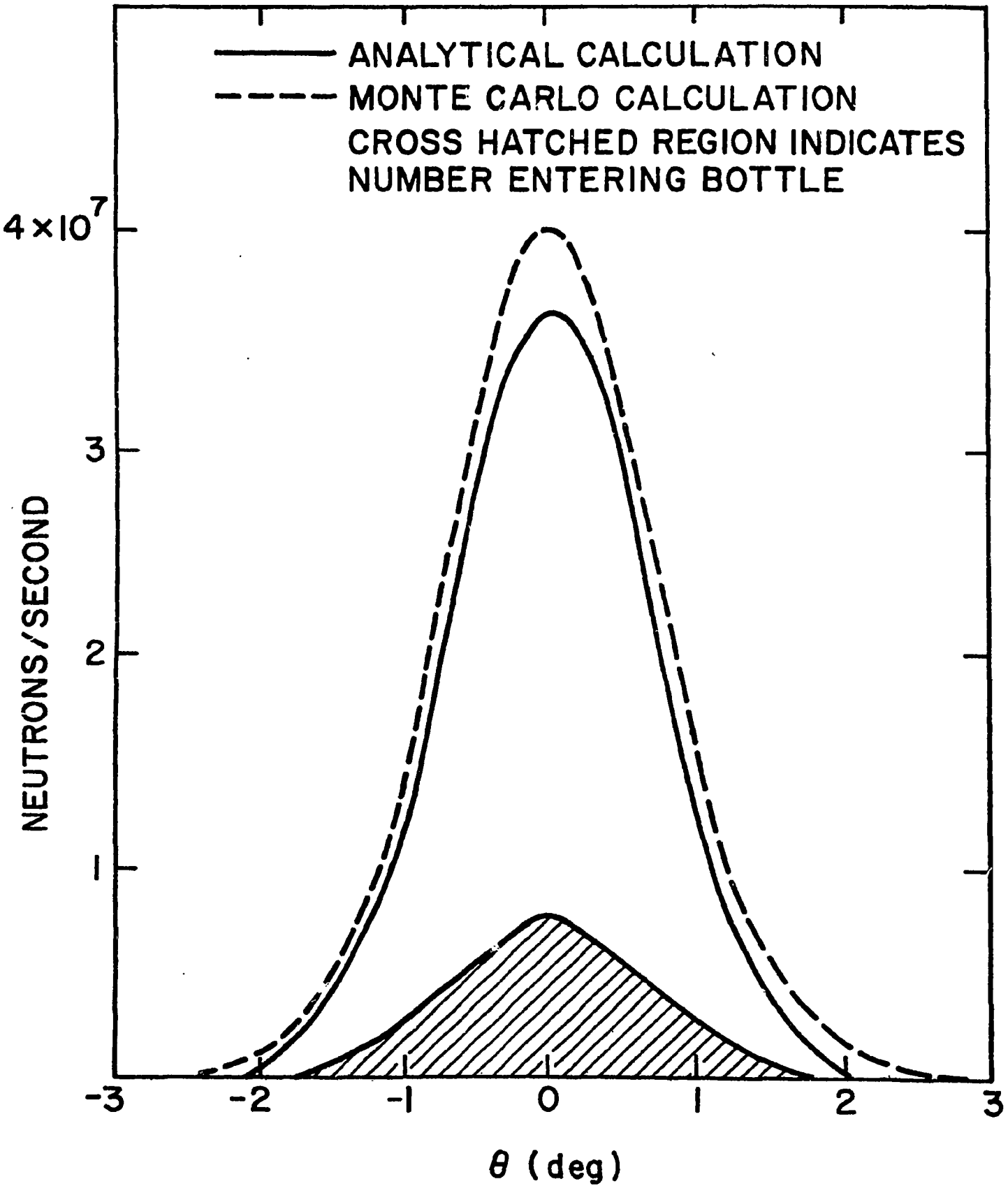
ANALYTICAL CALCULATION
MONTE CARLO CALCULATION
CROSS HATCHED REGION INDICATES
NUMBER ENTERING BOTTLE
4×10^7
3
2
1
NEUTRONS/SECOND
-3
-2
-1
0
1
2
3
θ (deg)

Fig. 6

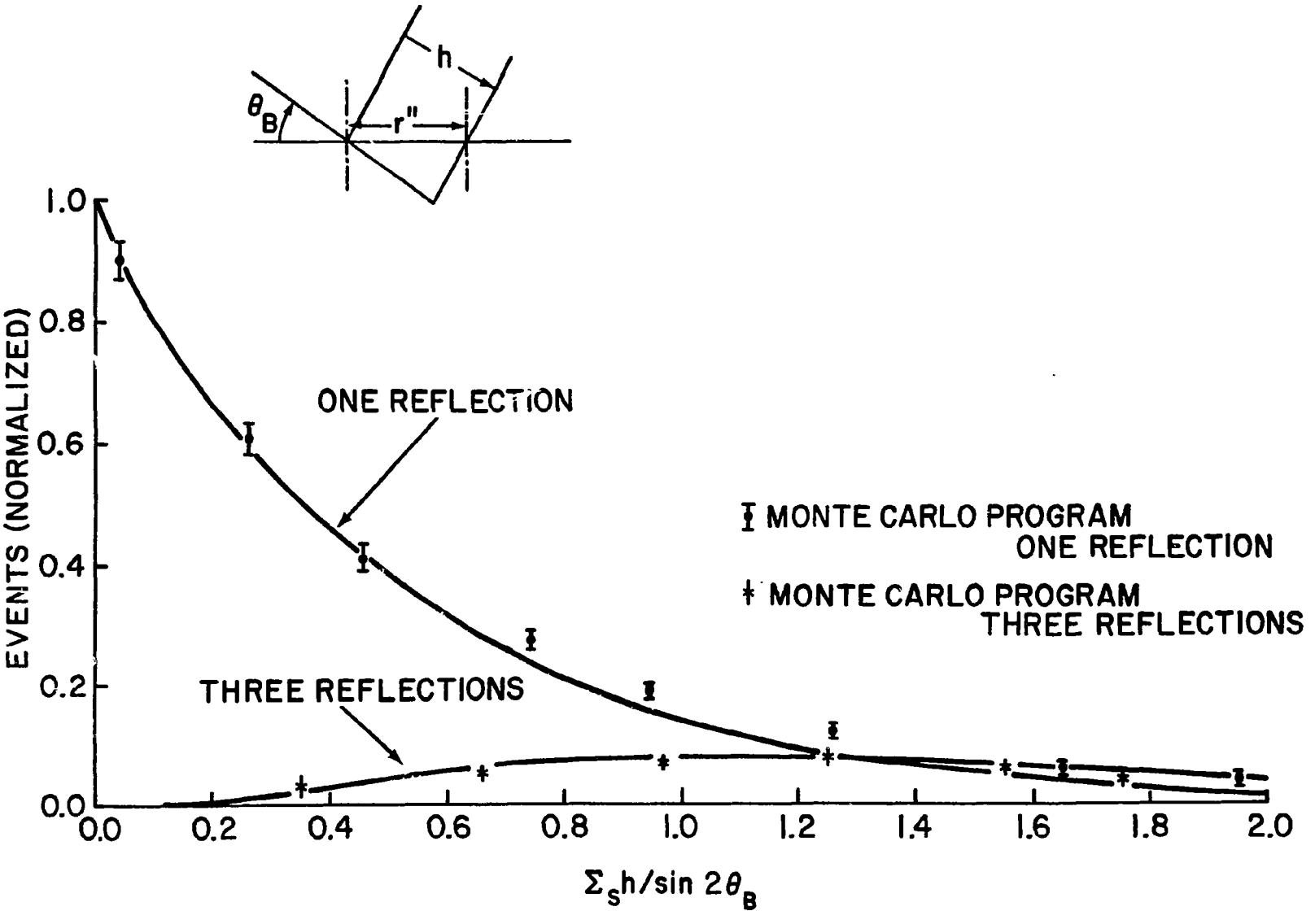
h
θ_B
r''
1.0
0.8
0.6
0.4
0.2
0.0
EVENTS (NORMALIZED)
ONE REFLECTION
THREE REFLECTIONS
MONTE CARLO PROGRAM
ONE REFLECTION
MONTE CARLO PROGRAM
THREE REFLECTIONS
0.0
0.2
0.4
0.6
0.8
1.0
1.2
1.4
1.6
1.8
2.0
$\Sigma_s h/\sin 2\theta_B$

Fig. 7.

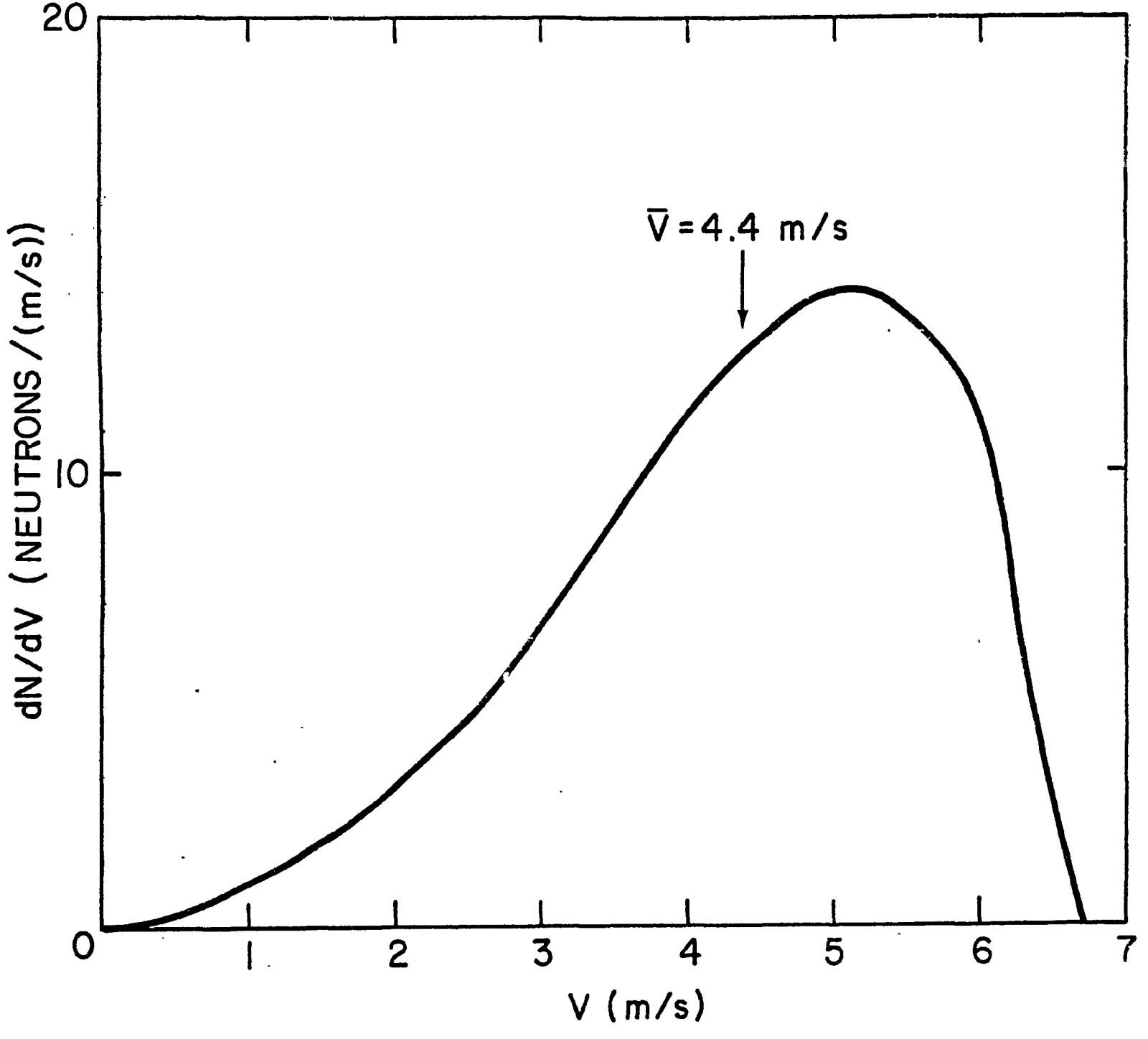

Fig. 8

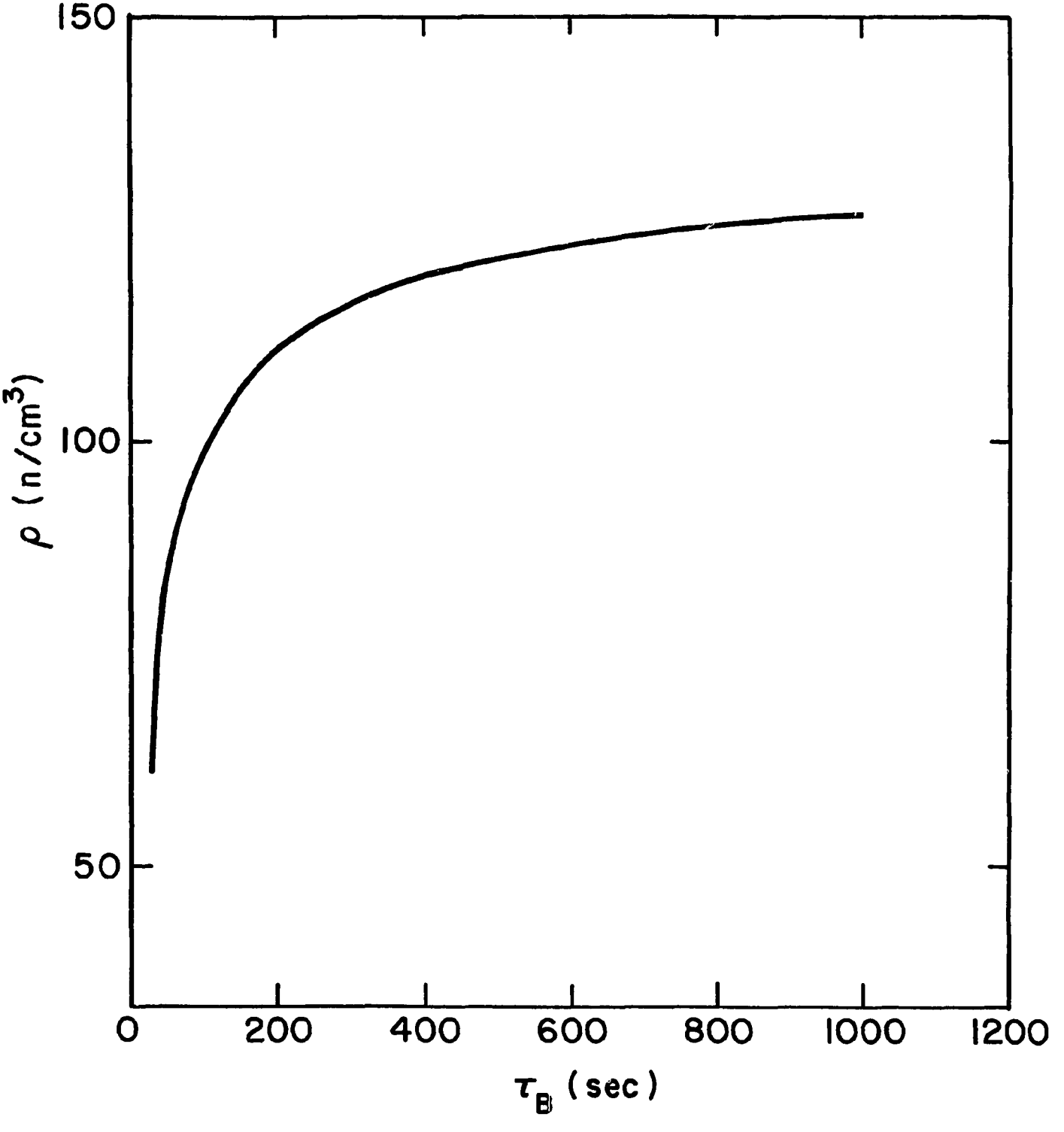

Fig. 9.

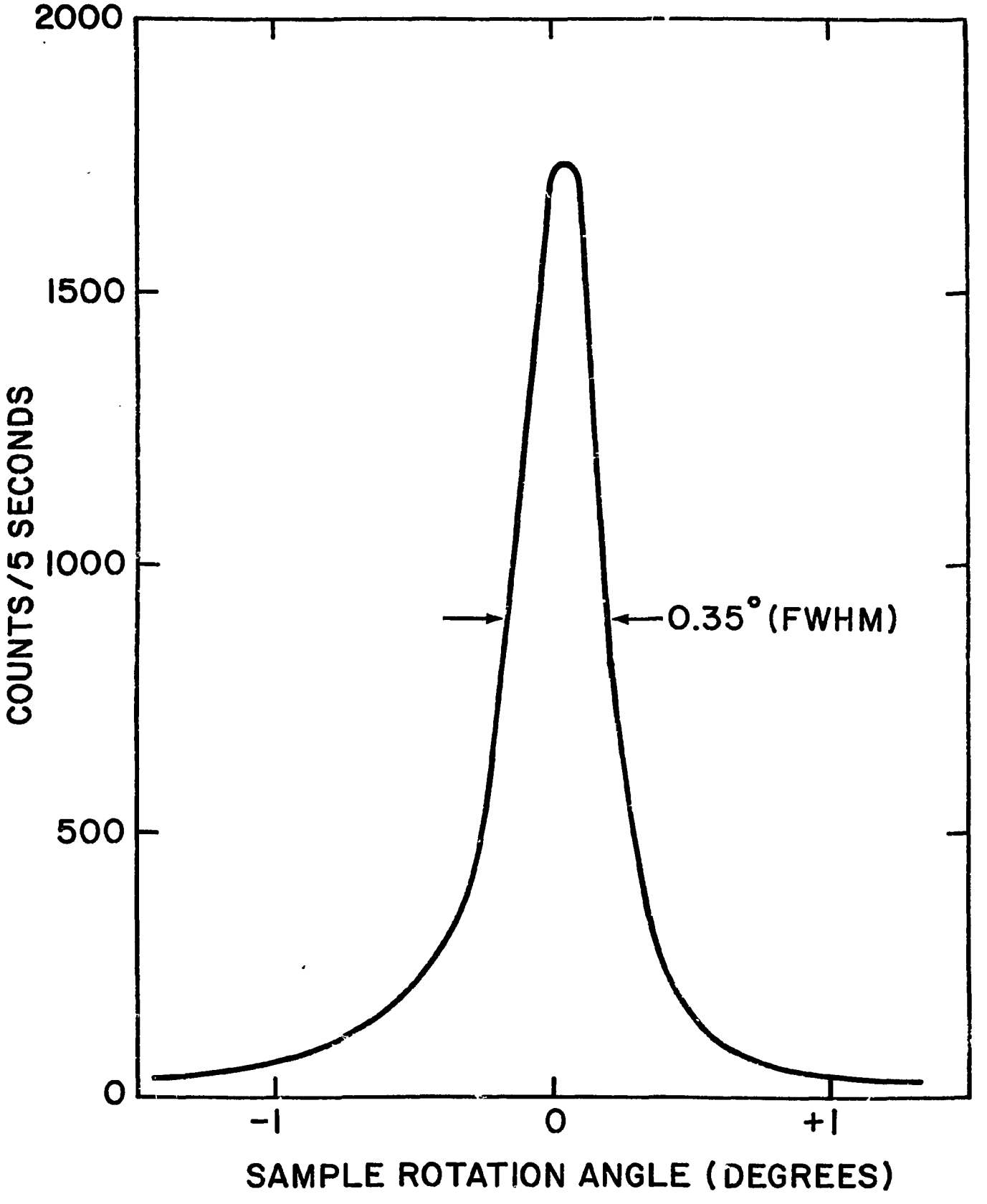
2000
1500
1000
500
0
COUNTS/5 SECONDS
0.35° (FWHM)
-1
0
+1
SAMPLE ROTATION ANGLE (DEGREES)

Fig. A1.

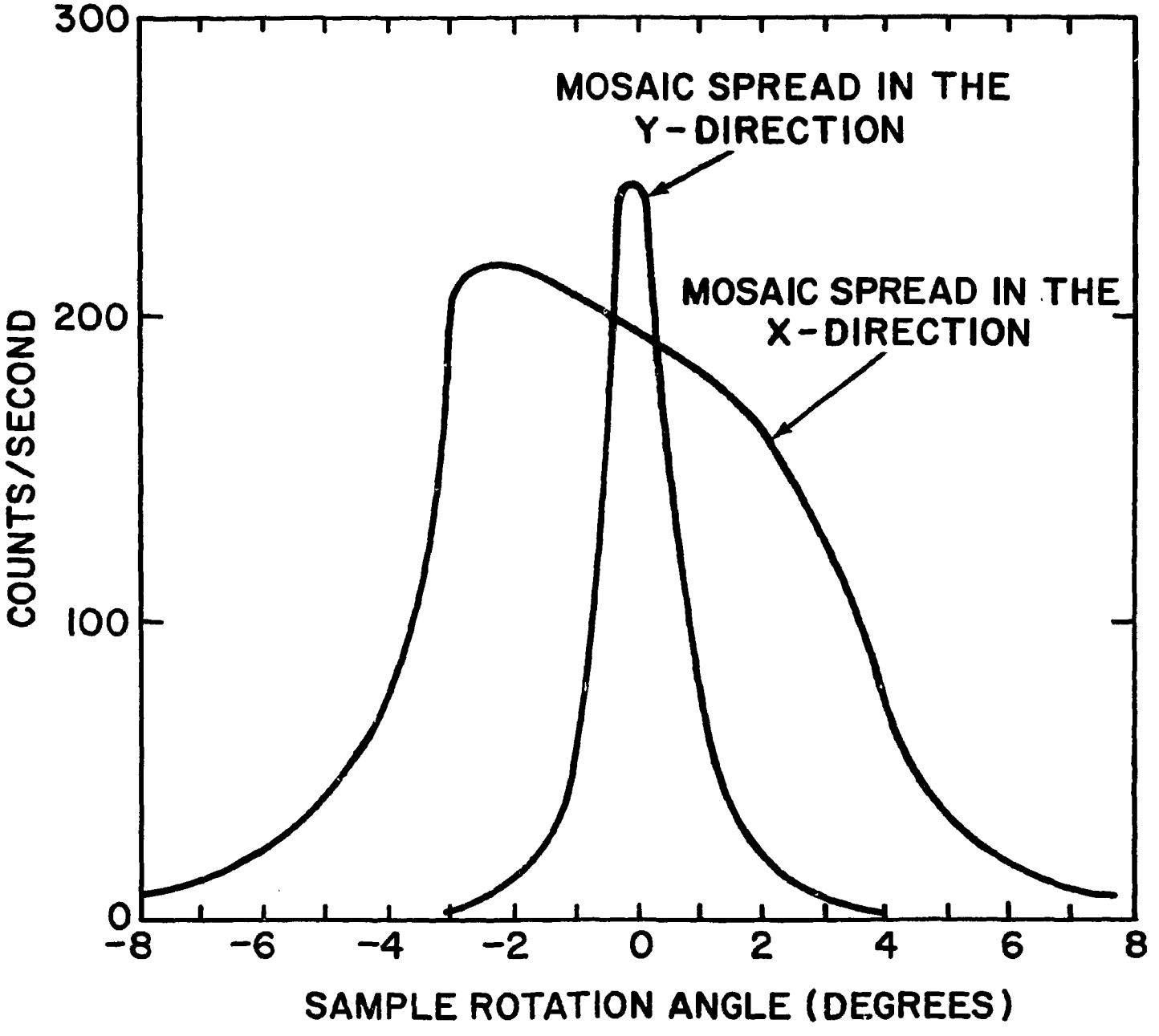
300
200
100
0
COUNTS/SECOND
MOSAIC SPREAD IN THE
Y-DIRECTION
MOSAIC SPREAD IN THE
X-DIRECTION
-8
-6
-4
-2
0
2
4
6
8
SAMPLE ROTATION ANGLE (DEGREES)

Fig. A2.